An-Najah National University

Faculty of Graduated Studies

Production of Useful ZnSe nano-film Electrodes By Electrodeposition onto Conducting Glass and Plastic Substrates

By

Heba Mohannad Mohammad Ghannam

Supervisor

Prof. Hikmat Hilal

Co-Supervisor

Dr. Ahed Zyoud

This Thesis is Submitted in Partial Fulfillment of the Requirements for the Degree of Master of Science in Chemistry, Faculty of Graduate Studies, An-Najah National University, Nablus, Palestine.

2021

Production of Useful ZnSe nano-film Electrodes by Electrodepostion Onto Conducting Glass and Plastic Substrates

By

Heba Mohannad Mohammad Ghannam

This Thesis was Defended Successfully on 14/06/2021 and approved by:

Defense Committee Members	Signature
– Prof. Hikmat S. Hilal / (Supervisor)	.....
– Dr. Ahed Zyoud / (Co. Supervisor)	.....
– Dr. Abdel-Rahman Abu Labdeh/ (External Examiner)	.....
– Dr. Maen Shtaiwi / (Internal Examiner)	.....

Dedication

To my beloved parents who brought me to the highway...

To my fiancée ...

To all of my family members…...

To all my friends……

To my distinguished teachers and everyone who contributed to my education….

Acknowledgements

First and foremost, I thank and praise Allah Almighty, who give me the blessing and strength to complete this study. I would like to express my deep gratitude to my supervisors Prof. Hikmat Hilal and Dr. Ahed Zyoud for their invaluable supervision, patience, support and helpful criticism of this research study.

Thanks also to the technical staff in the laboratories in the chemistry department at An-Najah National University. I also would like to thank Mr. Nafiz Dweikat for his technical help.

I would like to extend my sincere thanks to my thesis committee members Dr. Abdel-Rahaman Abu-Labdeh and Dr. Maen Shtawi for the nice discussion.

I also thank my friends for their support and help during this research.

Thanks also to Dr. Samer Zyoud, (AlAin, UAE), for his help in SEM and XRD measurements.

Finally, I would express my appreciation to my family for their support and encouragement through my study.

Heba M. M. Ghannam

الإقرار

أنا الموقع أدناه مقدم الرسالة التي تحمل العنوان:

Production of Useful Znse Nano-Film Electrodes By Electrodepostion Onto Conducting Glass and Plastic Substrates

انتاج أفلام نانوية مفيدة من ZnSe بالترسيب الكهربائي على شرائح الزجاج والبلاستيك المفيدة

أقر بأن ما اشتملت عليه هذه الرسالة هو نتاج جهدي الخاص، باستثناء ما تمت الاشارة اليه حيثما ورد، وأن هذه الرسالة ككل أو أي جزء منها لم يقدم من قبل لنيل أي درجة أو لقب علمي أو بحثي لدى أي مؤسسة تعليمية أو بحثية أخرى.

Declaration

The work provided in this thesis, unless otherwise referenced, is the researcher's own work, and has not been submitted elsewhere for any other degree or qualification.

Student's name: **اسم الطالب:**

Signature: **التوقيع:**

Date: **التاريخ:**

Table of Contents

List of Table

List of Figures

List of Abbreviation

Symbol	Abbreviation
E_{bg}	Energy band gap
CB	Conduction band
VB	Valance band
eV	Electron volt
SCs	Semiconductors
PEC	Photo-electrochemical cell
PV	Photovoltaic
E_f	Fermi energy level
E_c	Conduction band energy
E_V	Valance band energy
E_{redox}	Redox energy level
ECD	Electrochemical deposition
ITO	Indium doped tin oxide
MWCNTs	Multi Walled carbon nano tubes
FTO	Fluorine doped tin oxide
V_{OC}	Open-circuit potential
J_{SC}	Short circuit current density
FF	Fill Factor
J-V	Current density potential
η	Conversion efficiency
XRD	X-ray diffraction
SEM	Scanning electron microscope

Production of Useful Znse Nano-Film Electrodes By Electrodeposition Onto Conducting Glass and Plastic Substrates

By

Hiba Mohannad Mohammad Ghannam

Supervisor

Prof. Hikmat S. Hilal

Co-Supervisor

Dr. Ahed Zyoud

Abstract

ZnSe thin film electrodes have been deposited on two types of transparent conducting substrates, fluorine doped tin oxide (FTO) coated glass and indium doped tin oxide (ITO) coated plastic sheets, by electrochemical deposition (ECD). The prepared thin films have then been characterized by various techniques (X-ray diffraction (XRD), scanning electron microscopy (SEM) and electronic absorption spectra). Effects of deposition time, annealing temperature (100 °C and 150 °C under an inert gas), cooling rate (quickly and slowly cooled) and modification with MWCNTs film PEC characteristics, have been investigated. The ZnSe thin films have p-type conductivity as confirmed by PEC measurements.

XRD measurements show that ZnSe/FTO/glass thin films exist in mixed hexagonal and cubic phases, while the ZnSe/ITO/plastic has hexagonal phase only. The electronic absorption spectra for the films deposited on FTO/glass showed band gap values between (2.4-2.6 eV), while for films deposited on ITO/plastic, the band gap values are between (2.82-3.05eV).

The band gap value decreases with higher annealing temperatures. Rapidly cooled films show higher band gap than slowly cooled ones.

The films deposited on FTO/glass give higher conversion efficiency (0.84%) than the films deposited on ITO/plastic (0.087%). Annealing the ZnSe thin films lowered their PEC characteristics. Effect of using multiwalled carbon nanotube (MWCNT) layers onto ZnSe/FTO/Glass electrodes has been investigated. The MWCNT layer has been introduced by two different methods: by insertion between the ZnSe and the FTO layers (ZnSe/MWCNT/FTO/Glass), or by coating the ZnSe with MWCNT (MWCNT/ZnSe/FTO/Glass). The ZnSe/MWCNT/FTO/glass shows higher conversion efficiency (1.68%) compared to (0.84%) for ZnSe/FTO/Glass electrode. In this case, the MWCNT layer behaves as a charge transfer agent between the ZnSe layer and FTO substrate. The MWCNT/ZnSe/FTO/glass electrode exhibits lower conversion efficiency (0.61%). This is possibly due to the ability of MWCNT coating to block the incident light from reaching the surface of ZnSe.

Chapter one

Introduction

1.1 Solar Energy

To overcome climate and environmental change people started using renewable energy sources. Unlike fossil fuels, Renewable energies do not emit carbon dioxide or nitrogen dioxide gases. Solar radiation is one major renewable energy source [1-3].

Sun radiates electromagnetic radiations that are important for life. The solar radiation that reaches our Earth surface has ~8% ultraviolet, ~42.3% visible and ~49.4% infrared radiations [4].

Solar energy is renewable and sustainable with no negative effects to environment it can be used for heating and for electricity by solar cells [5-7]. Solar cells use semiconductor materials light-to-electricity conversion.

1.2 Semiconductors

Semiconductors are materials with lower conductivity than conductors (such as Cadmium) and higher conductivity than insulator (such as glasses). Semiconductors are useful in various technologies such as temperature sensors, mobile phones, computers, refrigerators and solar cells [8].

Materials are classified conductors, semiconductors and insulator based on their band gap values. Conductors have no band gap while Insulators have large band gaps, which require higher energy to transfer electricity.

Semiconductors have a small band gap values which allows thermal excitation of electrons between valence and conduction bands at moderate temperatures, Figure (1.1) [9,10].

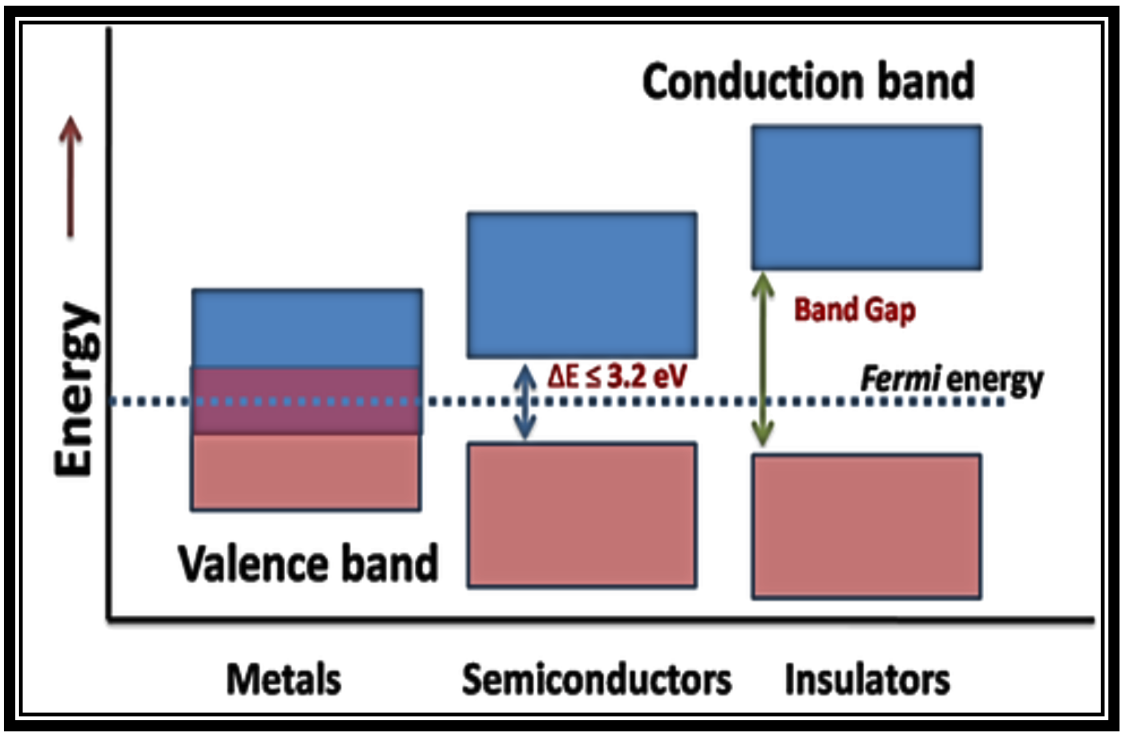

Figure 1.1: Band gap in conductors, semiconductors and insulators [11].

1.3 Semiconductors in Solar Cells

Semiconductors can be elements (as silicon and germanium) [12], II-VI and III-V compounds (as cadmium selenide and gallium phosphate), respectively [12, 13]. Oxides (zinc oxide) [14], ternary compounds ($CuInS_2$) [15] and quaternary compounds (Cu_2NiSnS_4) [16] are also known semiconductors.

1.4 Types of Semiconductors

Semiconductors (SCs) are classified into two groups, intrinsic SCs and extrinsic SCs.

1.4.1 Intrinsic SCs

Intrinsic semiconductor are pure (undoped) semiconductors which behaves as insulator at zero Kelvin. At higher temperatures, some electrons are thermally excited to conduction band, leaving holes in valence band, Figure (1.2). In this type the concentration of electron carriers is equivalent to the concentration of holes carriers [17-18].

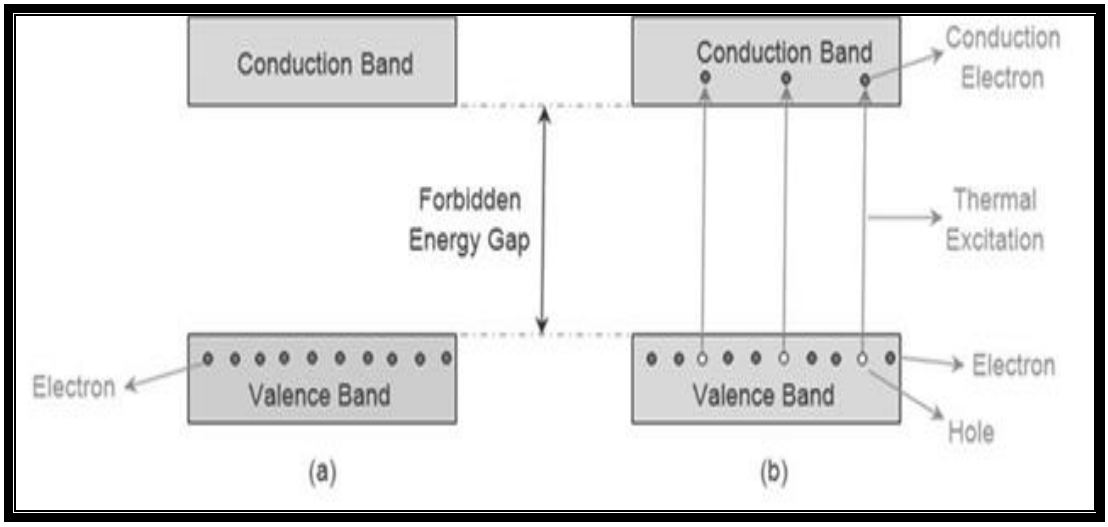

Figure 1.2: Energy band gap diagram of intrinsic semiconductor at (a 0 K and b) higher temperatures [19].

1.4.2 Extrinsic SCs

Extrinsic semiconductors are doped with impurities. Dopants are usually elements from III and V of the periodic table. Extrinsic semiconductors are two types [17]:

1.4.2.1 n-type

In this type the dopant atoms behave as electron donor, (like phosphorous and arsenic donors in silicon). P and As atoms have five electrons in the outer shells with energy level close to the Si conduction band. Electrons

can easily jump to the conduction band and behave as majority carriers, and the conduction is called negative type (n-type) [17,20,21], Figure (1.3a).

1.4.2.2 p-type

In this type the dopant atoms are electron acceptors (such as boron and gallium in silicon). B and Ga have three electrons in their outer shells. The energy level is close to the valence band. In these materials, valence band electrons of silicon jump to the dopant atoms leaving holes in the valence band. This type is called positive type (P-type) [17,21], Figure (1.3b).

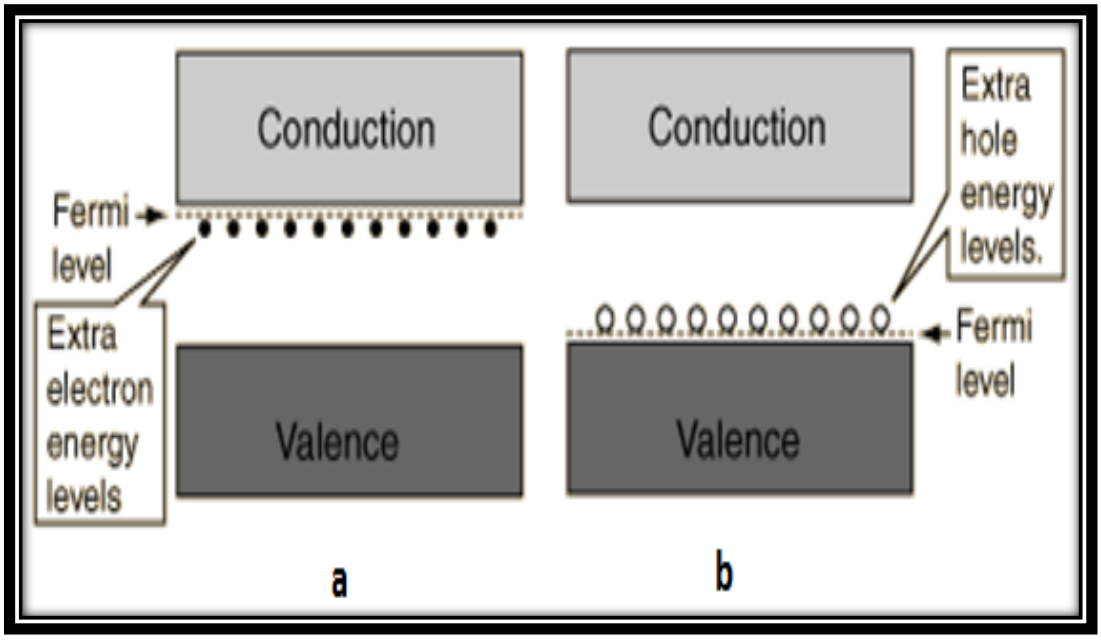

Figure 1.3: Extrinsic type semiconductor a) n-type SC and b) p-type SC [21].

1.5 Types of Solar Cells

There are two main techniques used to convert solar energy to useful electric energy. These main techniques are photovoltaic devices (PV) and photoelectrochemical solar cells (PEC).

1.5.1 Photovoltaic (PV) System.

PVs involve n-type and p-type semiconductors p-n junction. The p-n junction can be homojunction (same type of crystal) or a heterojunction (two different materials). Electron and hole pairs result from absorption of light in depletion layer, where electrons transfer to n-side and holes to the p-side, and photocurrent occurs, Figure (1.4) [22-24].

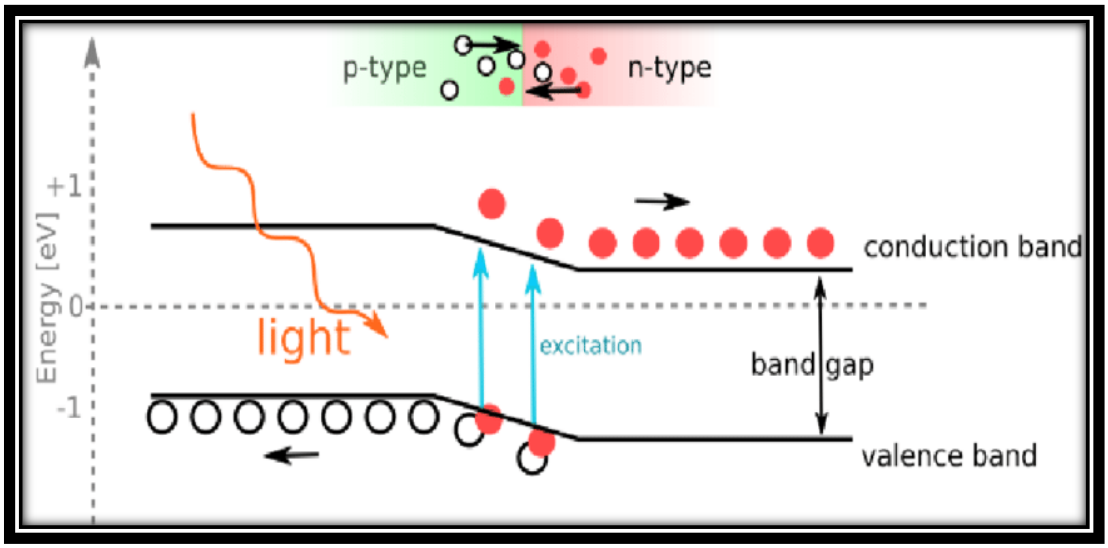

Figure 1.4: Formation of an electron-hole pair by absorbing light with frequency equal or higher than threshold frequency [24].

1.5.2 Photoelectrochemical (PEC) System

PECs can also transform light energy to electricity. PEC cells are based on the formation of SC/electrolyte junction. In n-type semiconductor, the Fermi level (E_f) is above the E_{redox} before equilibrium. The electrons therefore transfer from SC to electrolyte until the Fermi levels become equal. In p-type semiconductor the Fermi level of SC is below the Fermi level of electrolyte, and thus the electrons move from the electrolyte to the SC to reach equilibrium [23,25], Figure (1.5).

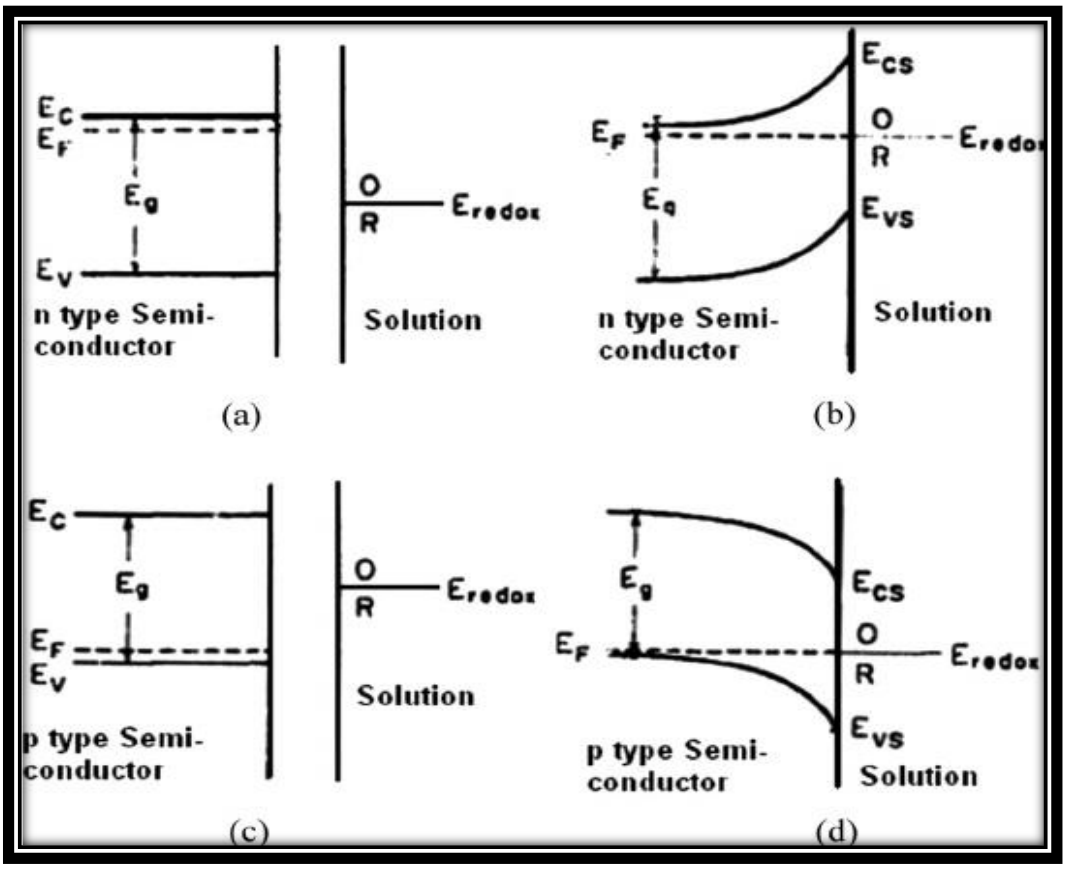

Figure 1.5: The energy schemes for n-type and p-type semiconductors in electrolyte solution before and after equilibrium [26].

1.6 Dark Current Generation in PEC Solar Cells.

In n-type SC, the dark current occurs when electrons transfer from the conduction band to electrolyte. At equilibrium there is a potential barrier that is generated by band bending in both valence and conduction bands. For transfer to occur the electrons must cross this barrier. Therefore the electrons need enough energy to overcome these barriers. A negative potential (ΔE_1) is therefore needed on the n-side. The space charge layer (SCL) disappears and flat band occurs, Figure (1.6) [20, 22].

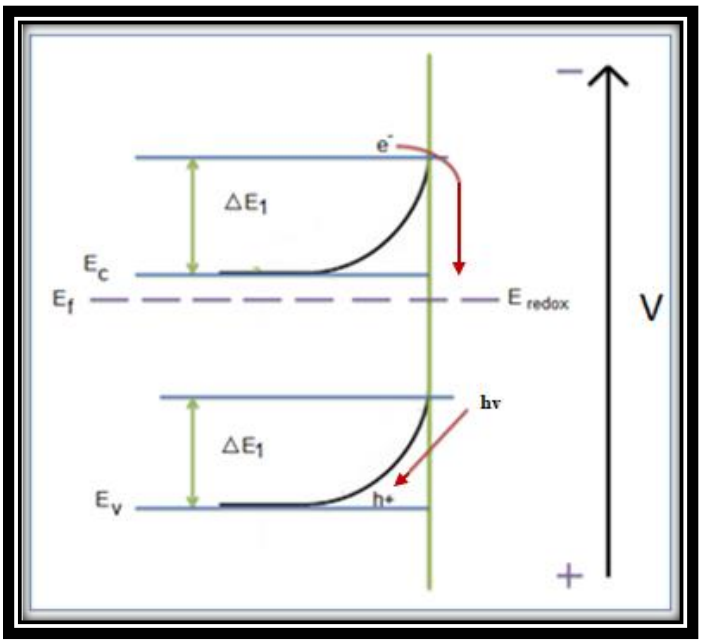

Figure 1.6:Dark current occurs in n-type SC [22].

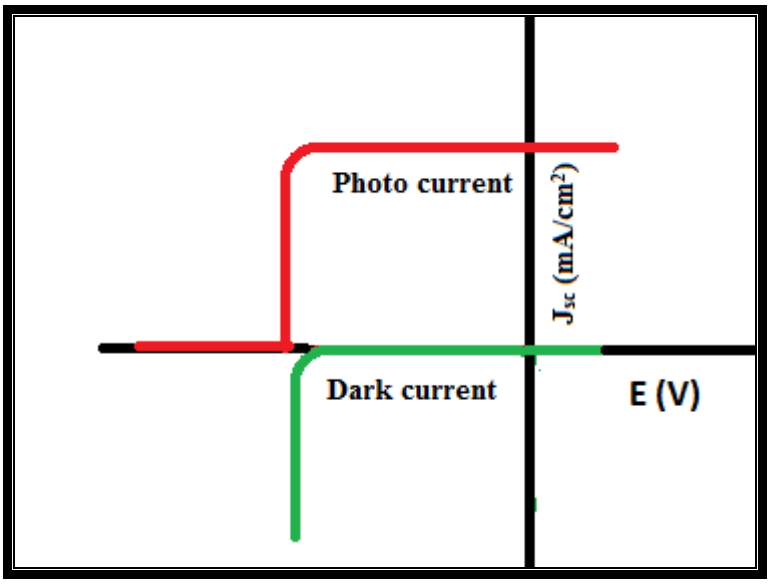

Figure 1.7: *J-V* plots for dark and photo current for n-type SC.

1.7 Photo Current Generation in PEC Solar Cells.

When photons with energy larger than E_{bg} of SC are absorbed, electrons and holes are created. The majority carriers (electrons in n-type and holes in p-type) concentrations and the minority carriers (holes in n-type and electrons in p-type) concentrations, photo current happen when the

electrode forms depletion layer and photo generated minority carriers migrate toward the electrode electrolyte interface, Figure (1.8) [27-29].

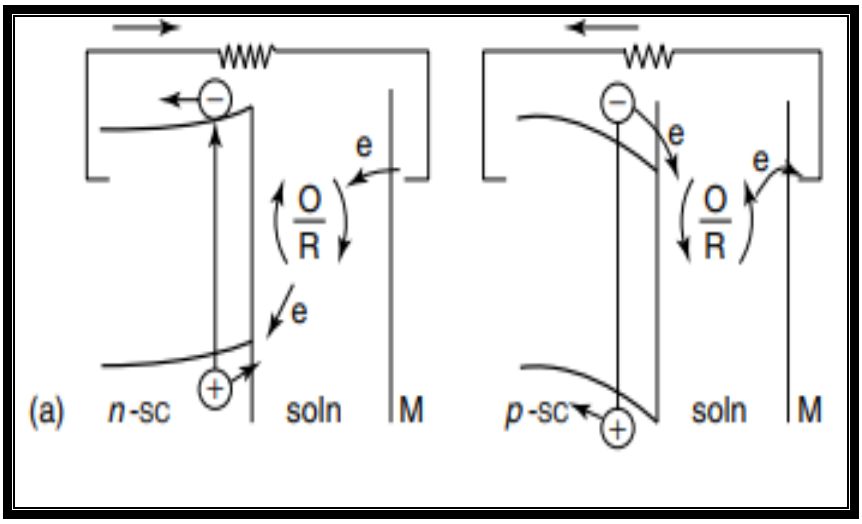

Figure 1.8: photo current generation at n-type and p- type SCs [30].

1.8 Thin Film Technology.

Thin film semiconductor electrodes are rapidly emerging this is due to their cost effectiveness and ease of fabrication. Thin films are being widely used in solar cells, electronics and biosystems [30, 31].

Thin films can be deposited on metals, glass and other substrates. Many techniques are used for thin film deposition such as chemical bath deposition (CBD), physical vapor deposition (PVD), and electrochemical deposition (ECD) [31, 32]. Many inorganic semiconductors are used as a thin film, such as CdSe, CuSe, CuO, ZnSe, CdTe and others.

1.9 ZnSe Thin Film.

Zinc Selenide (ZnSe) is semiconductor with a wide range of applications such as IR detectors, photoresistors, photovoltaics and photoelectrochemical

devices. It can be used as a window layer in heterojunction solar cells instead of CdS in CdS/CdTe solar cells because it is less toxic than CdS, also it can be used for photocatalytic applications. Zinc Selenide is n-type semiconductor with a medium band gap value 2.7 eV. It exists in hexagonal and cubic crystal structures as illustrated in Figure (1.9) [33-37].

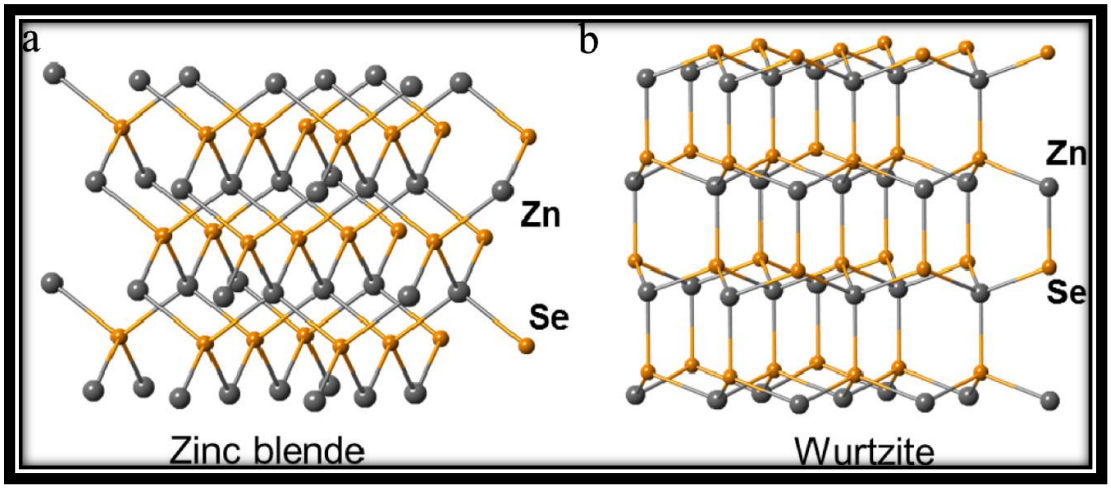

Figure 1.9: Crystal structure of ZnSe with (a) zinc blende and (b) wurtzite crystal structures [39].

ZnSe films can be deposited by various techniques, including chemical bath deposition [33, 34], electron beam evaporation [38], inert gas condensation method [36], electrochemical deposition [40] and physical thermal evaporation [36]. Among these methods Electrochemical deposition is simple, low cost and gives good contact layer on substrate [20, 40].

1.10 Objectives

The main objective of this work is to prepare ZnSe thin film onto fluorine doped oxide (FTO/glass) and indium tin oxide (ITO/plastic) by using electrochemical deposition technique (ECD). The electrode will be used in

photoelectrochemical (PEC) process. The prepared thin films will be modified by annealing, cooling rate and MWCNTs.

Technical objectives are:

1. Prepare ZnSe thin film electrode by using ECD onto FTO/glass and ITO/plastic. ECD method yields good contact between ZnSe and FTO, ITO surfaces.
2. Examine film efficiency in light-to-electricity conversion. Different characteristics (such as short circuit current density $\boldsymbol{J}_{sc}$, open–circuit photo potential $\boldsymbol{V}_{oc}$, conversion efficacy and fill factor) will be studied.
3. Examining the stability of the prepared ZnSe thin films to photo-degradation (photo corrosion) under PEC conditions.

1.11 Hypothesis

This work is based on the following assumptions:

1. Plastic is cheaper than glass. It is easier to move around and clean.
2. ECD makes good contact between ZnSe thin film and substrates.
3. Annealing the prepared ZnSe thin film is expected to give higher conversion efficiency compared to nonannealed ones.
4. Modifying the prepared ZnSe thin film with MWCNTs is expected to enhance efficiency and stability.

1.12 Novelty of this work.

1- Electrodeposition of ZnSe thin film on ITO/plastic has not been reported.

2- Effect of annealing temperatures and cooling rate on ZnSe thin film deposited on ITO/plastic will be studied here for the first time.

3- Effect of cooling rate on ZnSe thin film deposited on FTO/glass will be studied for the first time.

4- Modification of ZnSe thin film with MWCNTs for the PEC working electrode will be studied for the first time.

Chapter Two

Experimental

2.1 Materials

$ZnSO_4.7H_2O$, SeO_2 were purchased in pure form from Sigma-Aldrich. Acids were purchased from (SDFCL) in pure form, organic solvents were purchased from (Omega Raw- Materials CO.-Nablus), FTO/glass and ITO/plastic substrates were purchased from Sigma-Aldrich, and MWCNTs/Benzoic acid was kindly donated by Mrs. Heba Nassar, An-Najah National University.

2.2 Equipment

2.2.1 Electronic absorption spectrometer.

Solid state electronic absorption spectra of ZnSe thin films were measured using a Shimadzu UV-1601 spectrometer (at room temperature in the range 200-800 nm).

2.2.2 X-ray diffractometer (XRD).

ZnSe thin film crystallinity was investigated by a PAN alytical X'Pert PRO X-ray diffractometer (XRD) with CuKa (λ=1.5418 Å) as a source. XRD measurements were kindly conducted at the UAE University, Al-Ain, UAE. The XRD lines were identified by comparison with known JCPDS data-base cards.

2.2.3 Photoelectrochemical cell (PEC)

ZnSe thin film was used as working electrode (WE) in a PEC cell. Platinum sheet was used as counter electrode, and calomel electrode as internal reference. All electrodes were dipped in the redox couple solution. $K_3Fe(CN)_6/K_4Fe(CN)_6/LiClO_4$ system was used as a redox couple, with (0.1 M $K_3Fe(CN)_6$, 0.1 M $K_4Fe(CN)_6$, 0.1 M $LiClO_4$). N_2 gas (99.999%) was bubbled through the solution for (5-10) minutes to remove oxygen before each experiment and bubbling was then kept over the solution throughout experiments to minimize contamination, Figure (1.2).

Illumination was done with a 50-Watt halogen lamp with spectral range 450-800 nm. The illumination power on the electrode was ~0.0086 $W.cm^{-2}$.

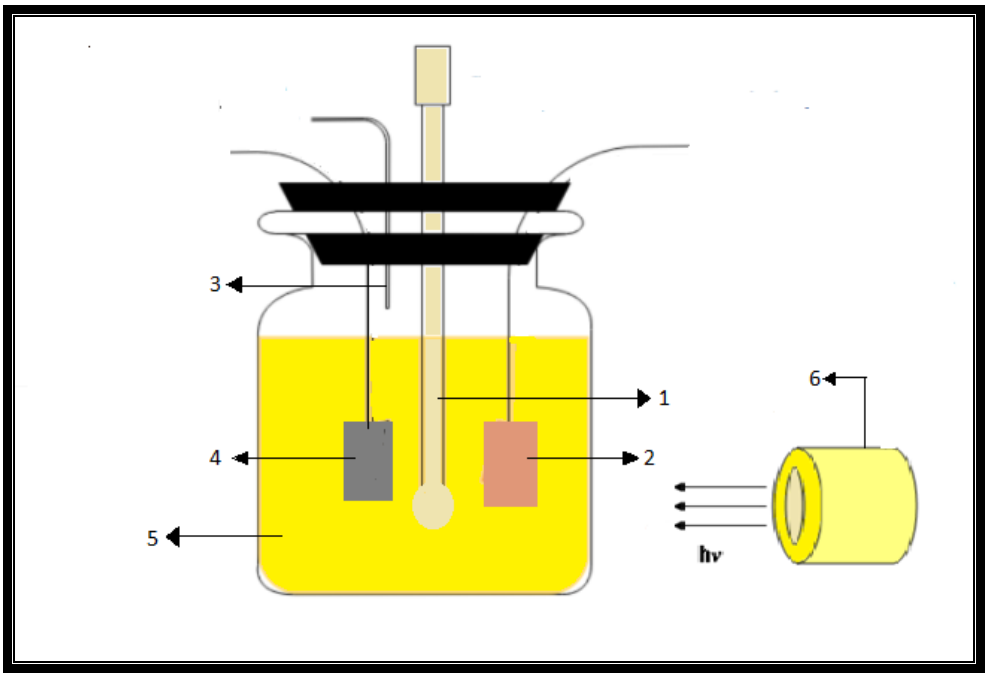

Figure 2.1: Schematic diagram for PEC measurement: 1) Internal reference electrode, 2) ZnSe thin film, 3) $N_{2(g)}$, 4) Pt counter electrode, 5) redox couple solution, 6) light source.

2.2.4 Scanning electron microscope (SEM)

SEM micrographs were recorded with a Field Emission Scanning Electron Microscope (FE-SEM, JEOL JSM-6700F) having an energy dispersive X-ray spectrometer (EDS). All SEM measurements were performed at the UAE University, Al-Ain, UAE.

2.3 FTO/glass substrate and ITO/plastic substrate cleaning

All FTO/Glass substrates were pre-cleaned prior to film deposition by washing with a detergent, and rinsing with distilled water. The substrates were then soaked in a sonicated acetone bath for 10 min, followed by isopropanol alcohol for more 10 min. Finally, the substrates were rinsed with distilled water and dried in air.

ITO/plastic substrates were cleaned by washing with a detergent then rinsed with distilled water and acetone. Finally, the substrates were rinsed with distilled water and dried in air.

2.4 Electrochemical deposition of ZnSe films

ZnSe were deposited on a pre-cleand FTO/glass or ITO/plastic substrate, which was used as working electrode (WE). The counter electrode (CE) was a Platinum sheet, and a calomel electrode was used as internal reference (RE).

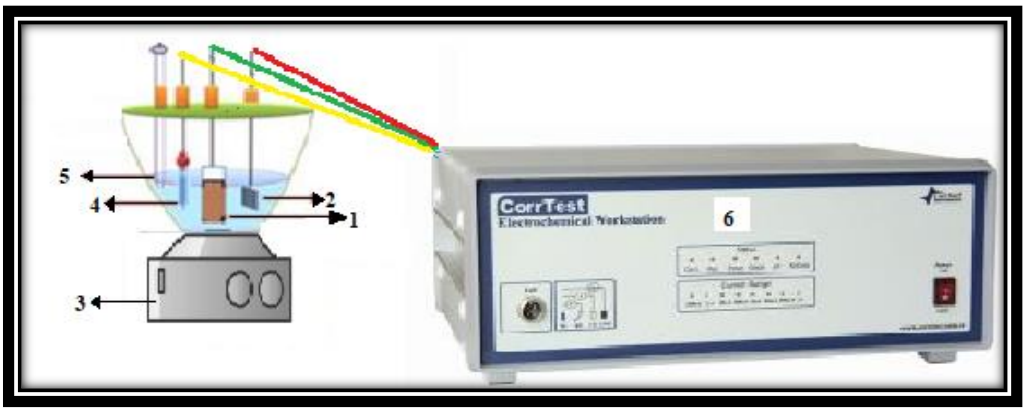

Figure 2.2: Schematic diagram for ECD ZnSe thin film. 1) ZnSe thin film 2)platinum counter electrode 3) magnatic stirrer plate 4) SCE 5) Nitrogen 6) potentiostat. [33]

ECD solution was prepared in an acidic solution containing $ZnSO_4$ and SeO_2. $ZnSO_4$ (30 ml, 0.2 M) was mixing with SeO_2 (30 ml, 0.002 M) and pH was adjusted to (2.5-3) by sulfuric acid addition [40].

Highly pure nitrogen was bubbled up inside the solution for 5 minutes before deposition to remove any dissolved oxygen. ZnSe thin film was grown by an applied potential of a DC stripping potential -0.9 V (vs SCE) at room temperature.

2.5 ZnSe thin film modification.

Various methods were used to modify the deposited ZnSe thin films such as: annealing process and cooling rate, in addition to modifying with MWCNTs.

2.5.1 Annealing.

Films were annealed using a Lindberg Heavy-Duty thermostated horizontal tube furnace. Annealing was performed at 100 °C and 150 °C under an inert gas for 10 min). The deposited ZnSe thin films were placed inside a

glass cylinder, which was inserted inside the oven under nitrogen atmosphere. Figure (2.3) describes the annealing system.

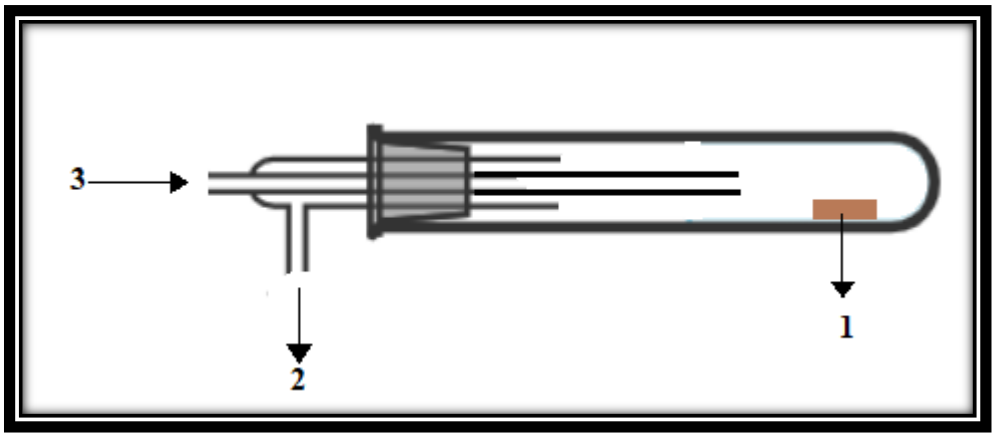

Figure 2.3:The annealing setup, 1) ZnSe thin film, 2) nitrogen outlet, 3) nitrogen inlet.

2.5.2 Cooling

2.5.2.1 Fast cooling (quenching)

After film annealing, the heated furnace was shut-off and the pyrex-glass cylinder (with ZnSe film inside) was taken out from the furnace and left to cool under an inert gas flow for 5-10 minutes.

2.5.2.2 Slow cooling

The heated furnace was shut-off and the film (inside the cylinder) was left inside the furnace to cool down to room temperature slowly (cooling rate of 0.8 $^{\circ}$C/min) under an inert atmosphere.

2.5.3 Modification of ZnSe with MWCNTs.

Pre-deposited ZnSe electrode was prepared by spray coating of MWCNTs/benzoic acid on pre-cleaned FTO/glass substrate, then annealing at 100 °C under Nitrogen atmosphere for 15 minutes and quickly cooled, after that ECD deposition of ZnSe.

Coated of ZnSe with MWCNTs was prepared by spray coating of MWCNTs/benzoic acid on ZnSe layer.

2.6 Current density vs. potential (J-V) plots

A Corr Test electrochemical workstation Potentiostat/Galvanostat was used to measure *J-V* plots. A 50-Watt halogen lamp was used to in photo-experiments

The redox couple was $K_3[Fe(CN)_6]/K_4[Fe(CN)_6]/LiClO_4$) . The short circuit current I_{sc} values were divided by the exposed area of the dipped electrode to obtain the values of the short circuit current density J_{sc}.

2.7 ZnSe thin film stability.

A Corr Test electrochemical workstation was used to measure the electrode stability. A potential of zero Volt (vs. calomel electrode) was applied, under steady illumination intensity of~ 0.0086 W/cm^2. The values of short circuit current density J_{sc} were measured with time. The short circuit current I_{sc} values were divided by the exposed area of dipped electrode to find the values of the short circuit current density J_{sc}.

Chapter three

Result and Discussion

Electrochemical deposition has been used to prepare ZnSe thin films on two different substrates (FTO/glass and ITO/plastic). Preparations have been made using various parameters to enhance the prepared films. Such parameters include deposition time (15, 30, 45 and 60 min), annealing (at 100 ºC and 150 ºC) under an inert gas for 10 min, cooling rate and modifying with MWCNTs.

The prepared thin films were characterized and investigated in terms of SEM, XRD, electron absorption spectra, EDX, J-V plots, efficiency and stability under photo-electrochemical conditions**.**

3.1 Characteristics of electrodeposited ZnSe/FTO/glass film

3.1.1 XRD Crystal Study

The XRD patterns of ZnSe/FTO/glass thin films before and after annealing are presented in Figure (3.1). The ZnSe films measured are polycrystalline cubic crystal having orientations of C(311) and C (400), and hexagonal structure having orientations H(100), H(002), H(101) and H(102). The films resemble those reported earlier [42-46]. The other peaks represent the FTO substrate and Selenium metal [42,47,48]. The selenium peaks are clearly shown in Figure (3.1) particularly in the film annealed at 150 °C with slow cooling.

The XRD data have been used to measure the particle size of ZnSe using Scherrer equation, $D = k\lambda/\beta\cos\theta$ [42]. The average grain sizes are

summarized in Table (3.1). The hexagonal structure exhibits relatively high sintering and crystalline growth by annealing. In the cubic phase the average particle sizes remain unchanged with no clear sintering at the used temperatures.

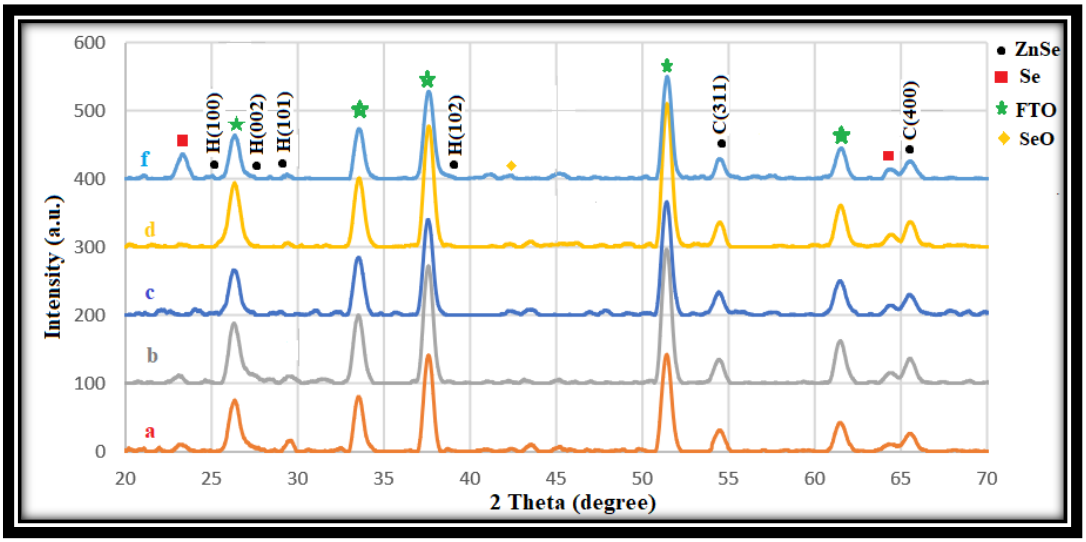

Figure 3.1: XRD patterns measured for ZnSe thin films electrodeposited on FTO/glass. a) non-annealed, b) annealed at 100 °C, quickly cooled, c) annealed at 100 °C and slowly cooled, d) annealed at 150 °C, quickly cooled and f) annealed at 150 °C, slowly cooled.

Table 3.1: The particle sizes of ZnSe/FTO/glass thin films.

Sample	Description	Average particle size for hexagonal structure (nm)	Average particle size for cubic structure (nm)
a	Non-annealed	35.32	14.80
b	Annealed at 100 °C, rapidly cooled	38.56	14.76
c	Annealed at 100 °C, slowly cooled	57.75	14.47
d	Annealed at 150 °C, rapidly cooled	53.44	14.21
f	Annealed at 150 °C, slowly cooled	63.13	15.36

3.1.2 Electronic absorption spectra.

3.1.2.1 The effect of deposition time on ZnSe/FTO/glass film electronic absorption spectra.

The electronic absorption spectra of the prepared ZnSe/FTO/glass thin films deposited in various deposition times are shown in Figure (3.2). The Figure shows that the highest electronic absorption spectrum is for the film prepared in 60 min due to its film thickness.

The results of Figure (3.2) are summarized in Table (3.2). The optical band gap values were determined by Tauc method [52] and the relationship of $\lambda_{bg}= 1240/E_{bg}$ [50]. The band gaps of the prepared ZnSe thin films are ranged between (2.4-2.6) which is less than optical band gap of ZnSe 2.7 eV. This band gap lowering may be attributed to the excessive Se in the films. Longer deposition time leads to increase in the film thickness and may lead to increased particle sizes. The band gaps therefore decreases as illustrated in Table (3.2).

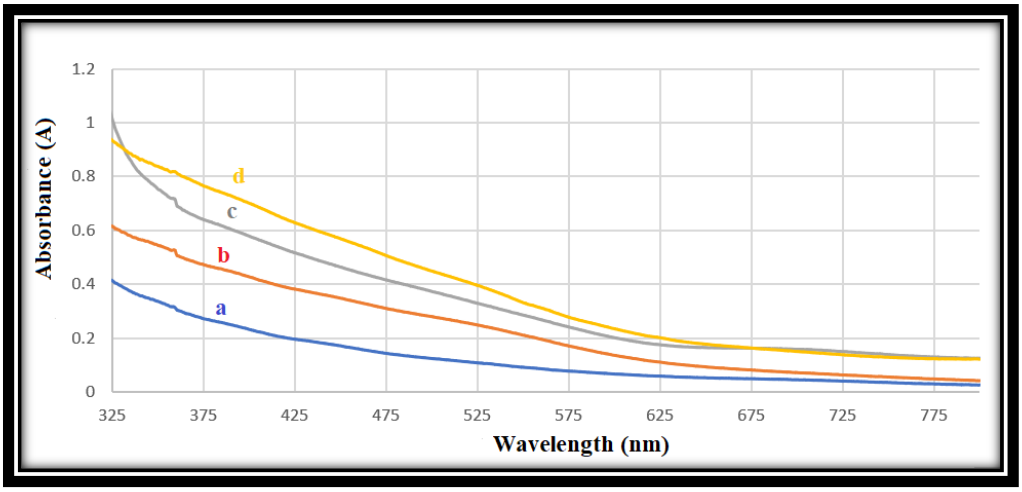

Figure 3.2: Optical absorption spectra measured for ZnSe/FTO/glass film in various time, a) 15 min b) 30 min c) 45 min and d) 60 min.

Table 3.2: Values of optical band gaps for ZnSe thin films deposited on FTO/glass in different times.

Sample	Deposition time (min)	E_{bg} (eV)	λ_{bg} (nm)
a	15	2.60	477
b	30	2.50	496
c	45	2.40	517
d	60	2.40	517

3.1.2.2 Effects of annealing temperature and cooling rate on electronic absorption spectra.

The prepared ZnSe/FTO/glass thin films were annealed at (100 °C and 150 °C) and then cooled either quickly and slowly. Figure (3.3) shows the electronic absorption spectra of the prepared ZnSe thin films annealed at (100 ºC and 150 ºC) and cooled at different rates (slow and fast). The Figure shows that the annealed films at 100 ºC have better absorption spectra than the non-annealed film. The annealed film at 100 ºC with slow cooling has better spectrum than the rapidly cooled film, which indicates that annealing at low temperature enhances the optical properties of ZnSe thin films. The films annealed at higher 150 ºC has lowest absorbance, due to effect of higher temperature on ZnSe thin film. Annealing may damage the thin film layers. In fact, the film layer partially disappeared during slow cooling, which indicates the lack of stability of the film. With slow cooling, the 150 ºC annealed film has enough time with higher temperature which allows film decomposition.

Table (3.3) summarizes the optical band gap and absorption band values. The band gap values are lowered in the annealed films due to increased particle sizes. The film annealed at 150 ºC gives lower band gap than the annealed films at 100 ºC, and the film annealed at 150 ºC with slow cooling gives the lowest band gap value. The particle size at higher temperature increases by sintering and leads to smaller band gaps. The annealed films cooled slowly are exposed to heat for a longer time, which causes more sintering.

As described above, slow cooling at 150 ºC has two effects on the film, decomposition and particle size increase. The results indicate the possibility to affect film properties simply by controlling annealing temperature and cooling rate, while avoiding higher temperature.

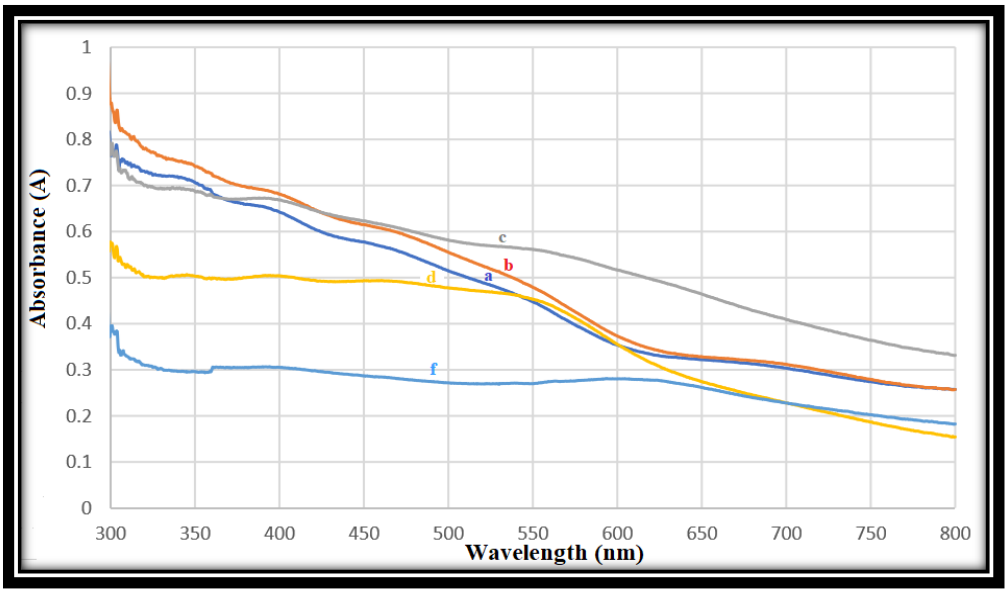

Figure 3.3: Optical absorption spectra measured for ZnSe thin film electrodes deposited on FTO/glass and a) non-annealed b) annealed (100 ºC) rapidly cooled c) annealed (100 ºC) slowly cooled d) annealed (150 ºC) rapidly cooled and f) annealed (150 ºC) slowly cooled.

Table 3.3: Effect of annealing and cooling rate on optical band gap for ZnSe/FTO/glass.

Sample	Description	E_{bg} (eV)	λ_{bg} (nm)
a	non-annealed	2.30	539
b	annealed at 100 ºC, rapidly cooled	2.28	544
c	annealed at 100 ºC, slowly cooled	2.10	590
d	annealed at 150 ºC, rapidly cooled	1.82	681
f	annealed at 150 ºC, slowly cooled	1.80	689

3.1.3 Photoelectrochemical (PEC) characteristics for ZnSe/FTO/glass thin film.

The photo-electrochemical characteristics of the prepared films have been measured. The photo J-V plots for films prepared under different conditions are measured.

3.1.3.1 Effect of deposition time on the J-V plots of ZnSe/FTO/glass films.

Photo J-V plots for thin films deposited in different times are shown in Figure (3.4). The plots show that the ZnSe films have p-type conductivity as illustrated in the Figure. Some literature showed that ZnSe is n-type conductor, while others showed p-type conductivity for the films [51, 52]. The p-type behavior is due to the increased ratio of selenium to zinc. The reddish color of the films is an evidence of an excess of elemental selenium as indicated in earlier report and as shown in XRD results [52]. Selenium element takes electrons from the crystal and becomes Se^{2-}, so that the shortage in electrons converts the crystal to a p-type.

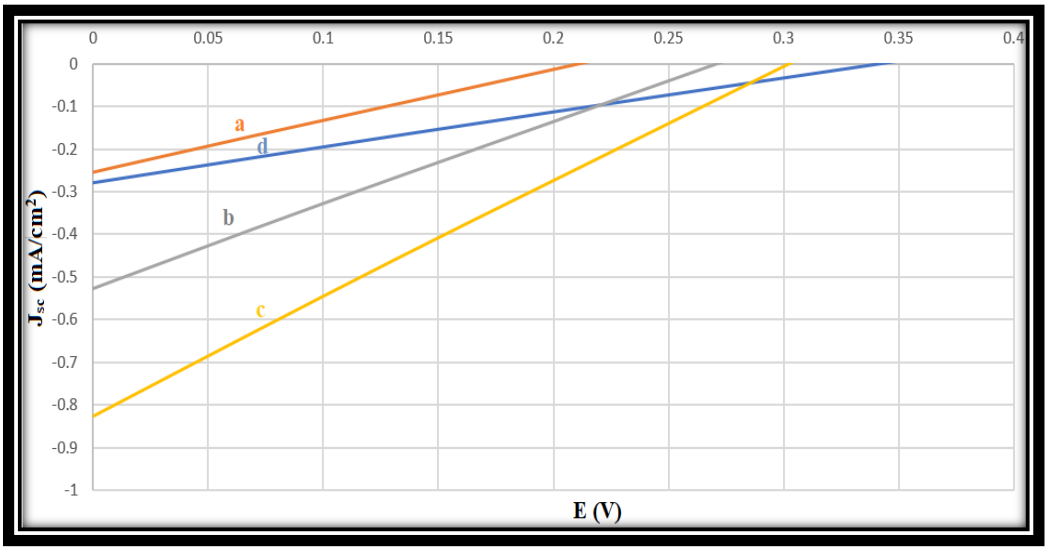

Figure 3.4: Photo J-V plots measured for ZnSe/FTO/glass films deposited in a) 15, b) 30, c) 45 and d) 60 min.

Table 3.4: PEC characteristics for ZnSe/FTO/glass film in different times.

Sample	Deposition time (min)	[a] V_{OC} (V)	[b] J_{SC} (mA/cm^2)	[c] η%	[d] FF%
A	15	0.21	-0.25	0.21%	28.6%
B	30	0.27	-0.51	0.45%	24.3%
C	45	0.30	-0.81	0.82%	25.7%
D	60	0.34	-0.28	0.32%	22.3%

[a] V_{OC} = *open-circuit voltage*

[b] J_{SC} = *short-circuit* current *density*

[c] η *(%) = conversion efficiency = [(maximum observed power density)/ (reach-in power density)] ×100%.*

[d] *FF = Fill factor = [(maximum observed power density)/*J_{sc}×V_{oc}*] ×100%.*

The prepared ZnSe film deposited in 45 min has highest V_{OC} (0.30), J_{SC} (-0.81) and efficiency (0.82%) among the series. The film prepared in 45 min has narrow band gap value, which means it can absorb light in wider visible range, which increases conversion characteristics.

3.1.3.2 Effects of annealing temperatures and cooling rate on J-V for ZnSe/FTO/glass thin films.

PEC properties for ZnSe thin film annealed at (100 ºC and 150 ºC) with different cooling rates (slow and fast) are measured**.** Photo J-V plots for thin films annealed at (100 ºC and 150 ºC) and cooled slowly and quickly are shown in the Figure (3.5). The results of the Figure are summarized in Table (3.5).

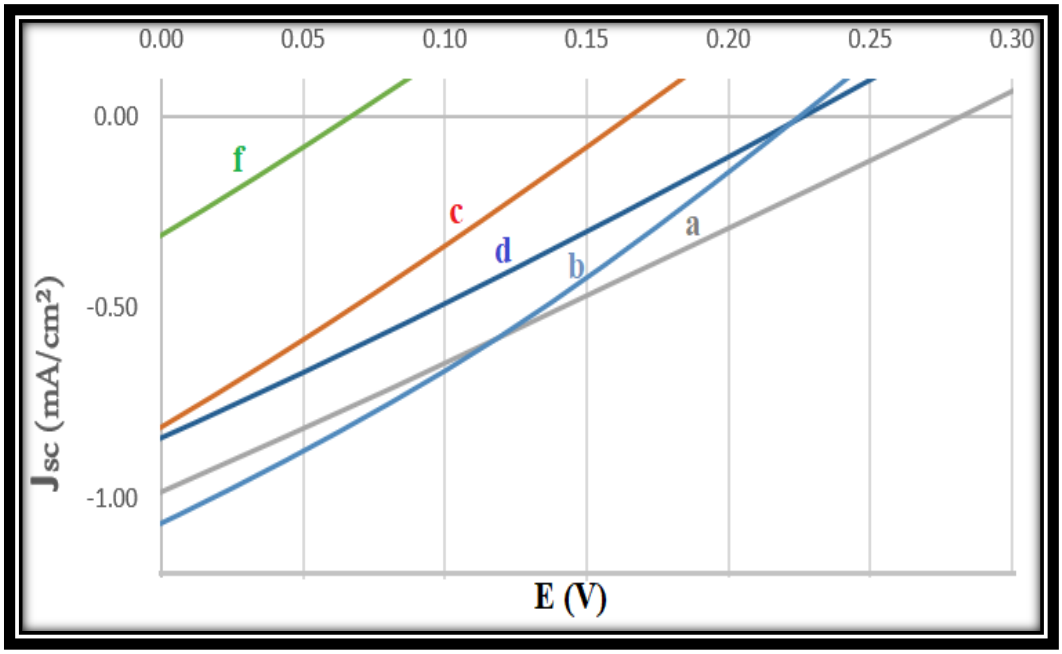

Figure 3.5: Photo J-V plots for ZnSe/FTO/Glass electrodes a) non-annealed, b) annealed at 100 ºC rapidly cooled c) annealed at 100 ºC slowly cooled d) annealed at 150 ºC rapidly cooled and f) annealed at 150 ºC slowly cooled.

Table 3.5: PEC characteristics for ZnSe/FTO/Glass thin film annealed at (100 ºC and 150 ºC) and cooling rate.

Sample	Description	$^{a}V_{OC}$ (V)	$^{b}J_{SC}$ (mA/cm^2	$^{c}\eta$%	^{d}FF%
a	non-annealed	0.28	-0.96	0.84%	25.6%
b	annealed at 100 ºC, quenched	0.24	-1.05	0.76%	27.5%

c	annealed at 100 ºC, slowly	0.17	-0.85	0.41%	25.1%
d	annealed at 150 ºC, quenched	0.22	-0.84	0.58%	26.7%
f	annealed at 150 ºC, slowly	0.08	-0.30	0.08%	33.8%

[a] V_{OC} = ***open-circuit voltage***

[b] J_{SC} = ***short-circuit* current *density***

[c] η ***(%) = conversion efficiency = [(maximum observed power density)/ (reach-in power density)] ×100%.***

[d] ***FF = Fill factor = [(maximum observed power density)/J_{sc}×V_{oc}] ×100%.***

The V_{OC} values for films annealed at (100 ºC and 150 ºC) and quickly cooled resemble each other. The annealed film at 100 ºC with quick cooling has highest J_{SC} value (-1.05). The non-annealed film has highest efficiency (0.84%). The film annealed at 100 ºC with quick cooling has higher efficiency (0.76%) than film annealed at 150 ºC (0.41%) and quickly cooled. Quick cooling gave higher efficiencies than slowly cooled films (0.41% and 0.08%) annealed at (100 ºC and 150 ºC) respectively. Here the efficiency result for annealed films at 100 °C did not agree with their electronic absorption spectrum, possibly due to the lowering of the Zn content through annealing.

Annealing may improve the crystallinity of the film and reduce surface roughness [52] but not all the time. Here the annealing doesn't enhance the photoelectrochemial properties of ZnSe thin film. The ECD layer is relatively uniform without annealing. Upon heating the kinetic energy increases, and leads to increased disorder in the film [53,54]. With rapid

cooling there will be less disorder in the crystal, while in slow cooling the crystals have longer exposure time to high temperature which causes more disorder. The deposited ZnSe film is partially destroyed by annealing at 150 °C and slow cooling, leading to sublimation of the Zn element, with longer exposure to heat.

3.1.4 SEM images for ZnSe/FTO/glass thin films.

SEM images have been measured for non-annealed and annealed films at 100° C with different cooling rates, Figure (3.6). The Figure shows agglomerations with nonuniform size distribution between (100-500) nm.

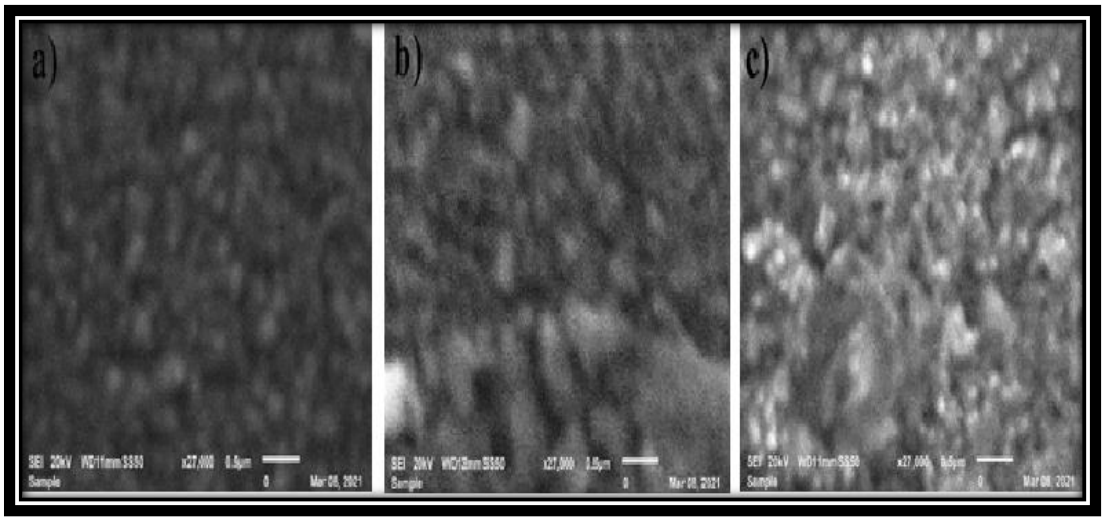

Figure 3.6: SEM images for ZnSe/FTO/glass thin films, a) non-annealed b) annealed at 100°, rabidly cooled and c) annealed at 100°, slowly cooled.

3.2 Characteristics of ZnSe films modified with MWCNTs

Two types of MWCNT modified ZnSe films have been deposited onto Glass/FTO substrates. In one type the Glass/FTO surface was first coated with MWCNT and the ZnSe thin films was then deposited. The resulting film is thus named (ZnSe/MWCNT/FTO/Glass). The other ZnSe thin film was prepared by depositing the ZnSe film onto the Glass/FTO substrate,

followed by coating with MWCNT layer. The resulting film is named (MWCNT/ZnSe/FTO/Glass).

3.2.1 XRD measurements for ZnSe thin films modified with MWCNTs.

The XRD patterns of ZnSe/FTO/glass thin films modified with MWCNTs are shown in Figure (3.7). The ZnSe thin films are polycrystalline with mixed cubic and hexagonal crystal phases. The ZnSe /MWCNTs /FTO /glass has higher crystallinity than other films. This is evidenced by comparing the C (311) and C(400) peaks with the FTO peaks. The average particle sizes have been measured by Scherrer equation, as described above, and are summarized in Table (3.6). The presence of MWCNTs is affected on the average particle size of ZnSe, in cubic phase the average particle size for ZnSe in case of ZnSe/MWCNTs/FTO/glass are relatively larger than others, while in hexagonal phase the average particle size for Naked ZnSe are relatively larger than others.

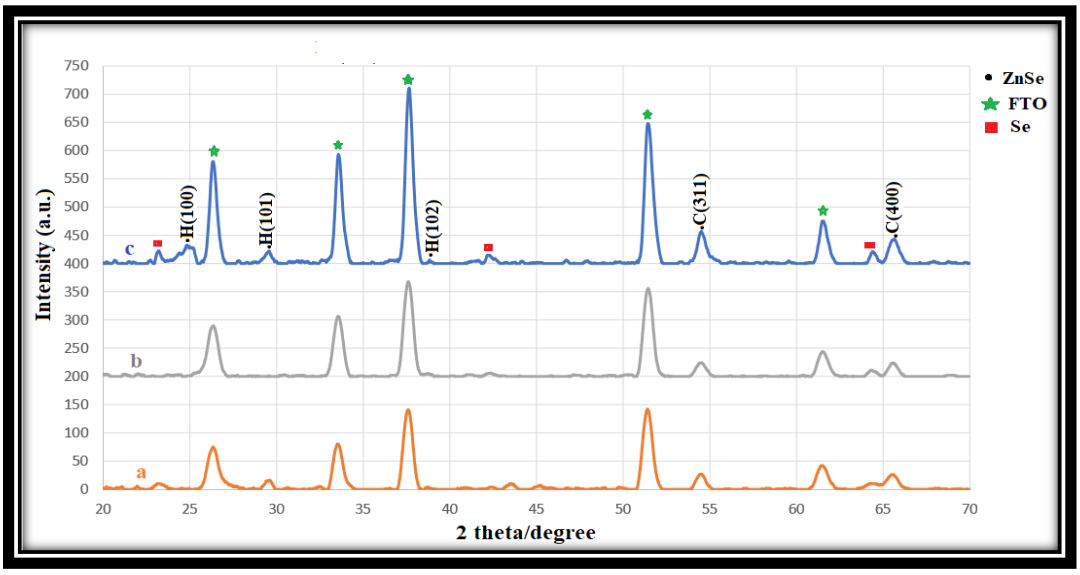

Figure 3.7: XRD patterns measured for ZnSe thin films electrodeposited on FTO/glass. a) ZnSe/FTO/glass, b) MWCNT/ZnSe/FTO/glass and c) ZnSe/MWCNTs /FTO/glass.

Table 3.6: The particle sizes of ZnSe modified with MWCNTs.

Sample	Description	Average Particle size in hexagonal structure (nm)	Average particle size in cubic structures (nm)
a	ZnSe/FTO/glass	35.32	14.80
b	MWCNTS/ZnSe/FTO/glass	31.43	15.26
c	ZnSe/MWCNTs/FTO/glass	33.44	17.41

3.2.2 Electronic absorption spectra.

The electronic absorption spectra of the prepared ZnSe thin films modified with MWCNTs are presented in Figure (3.8). Band gap values are shown in Table (3.7). Treatment with MWCNTs did not affect the electronic absorption spectra for ZnSe film.

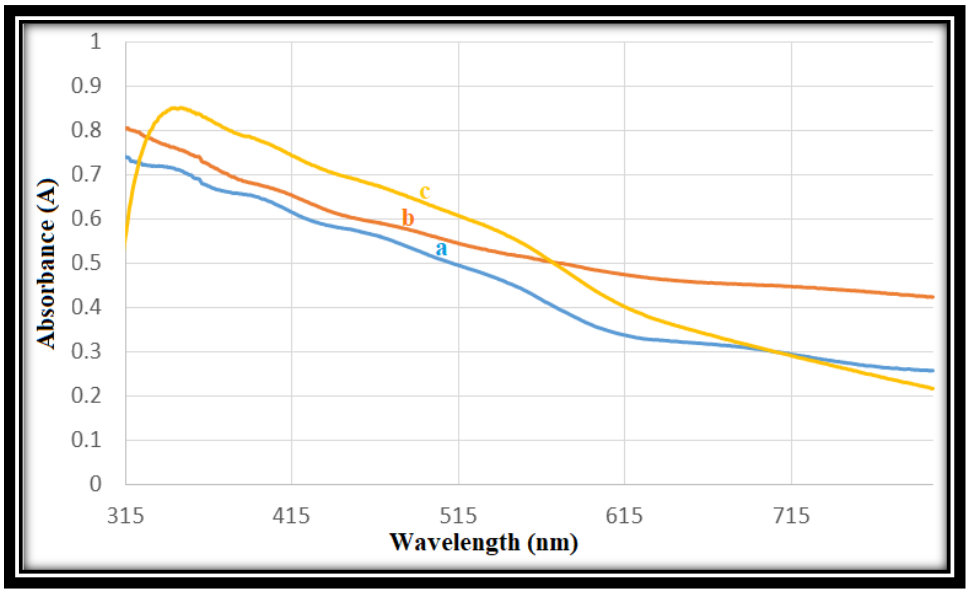

Figure 3.8: Optical absorption spectra measured for ZnSe thin film electrodes modified with MWCNTs, a) ZnSe/FTO/Glass, b) ZnSe/MWCNT/FTO/Glass and c) MWCNT/ZnSe/FTO/Glass.

Table 3.7: the optical band gaps and absorption bands for ZnSe thin film modified with CNTs.

Sample	Description	E_{bg} (eV)	λ_{bg} (nm)
a	ZnSe/FTO/Glass	2.33	532
b	ZnSe/MWCNT/FTO/Glass	2.30	539
c	MWCNT/ZnSe/FTO/Glass	2.17	571

3.2.3 *J-V* plots for MWCNT modified ZnSe films

The photo J-V plot is measured for the prepared thin films modified with MWCNTs as represented in Figure (3.9). The results of the Figure are summarized in Table (3.8).

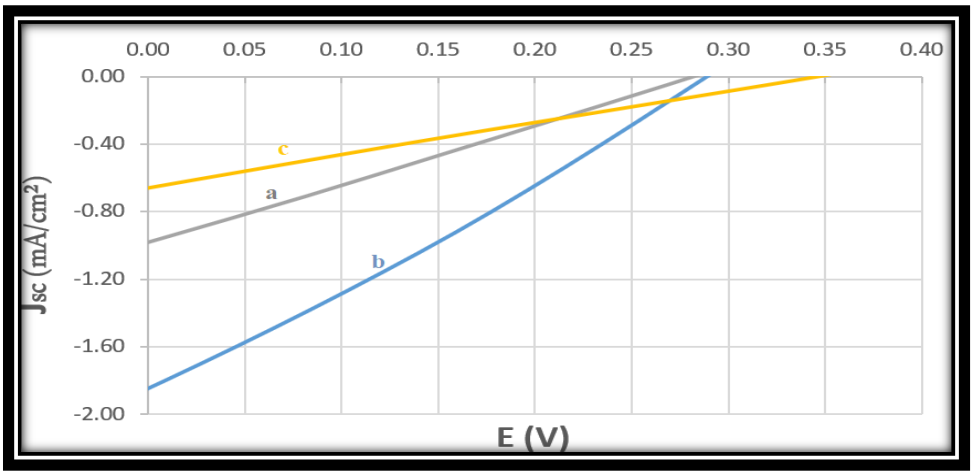

Figure 3.9: Photo J-V plots measured for various treated electrodes a) ZnSe/FTO /Glass, b) ZnSe/MWCNT/FTO/Glass and c) MWCNT/ZnSe/FTO/Glass.

Table 3.8: PEC characteristics for ZnSe thin films modified with CNTs.

Sample	Description	[a] V_{OC} (V)	[b] J_{SC} (mA/cm^2)	[c] η%	[d] FF%
a	ZnSe/FTO/Glass	0.28	-0.96	0.84%	25.6%
b	ZnSe/MWCNT/FTO/Glass	0.29	-1.85	1.68%	26.9%
c	MWCNT/ZnSe/FTO/Glass	0.33	-0.65	0.61%	23.3%

[a] V_{OC} = *open-circuit voltage*

[b] J_{SC} = *short-circuit* **current** *density*

[c] η *(%) = conversion efficiency = [(maximum observed power density)/ (reach-in power density)] ×100%.*

[d] *FF = Fill factor = [(maximum observed power density)/J_{sc}×V_{oc}] ×100%.*

The ZnSe/MWCNT/FTO/Glass electrode shows the highest conversion efficiency (1.68%), while the MWCNT/ZnSe/FTO/Glass film shows the lowest conversion efficiency (0.61%).

MWCNTs provides an effective way for holes to transfer from ZnSe to FTO. So it leads to enhanced PEC characteristic Figure (3.10 a). The CNT layer may enhance contact between the ZnSe layer and the FTO surface. The MWCNT/ZnSe/FTO/Glass with MWCNT coating shows lowered conversion efficiency. This is because the MWCNT coating blocks the light from reaching the surface of ZnSe. Moreover, the MWCNT layer increases resistance and slows charge transfer at the solid/electrolyte interface, as described in Figure (3.10 b).

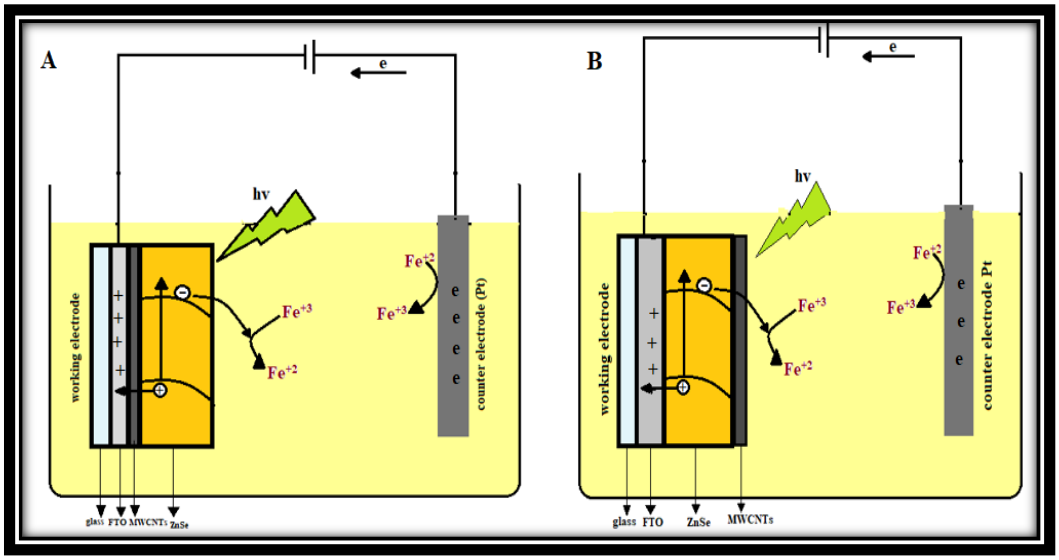

Figure 3.10: Effect of MWCNT on charge transfer process in A) ZnSe/MWCNT /FTO/Glass and B) MWCNT/ZnSe/FTO/Glass.

3.2.4 SEM images for ZnSe modified with MWCNTs.

SEM surface images have been measured for ZnSe thin films modified with MWCNTs, Figure (3.11). In MWCNT/ZnSe/FTO/Glass, The MWCNT particles can be observed at the surface of ZnSe Figure (3.11 b). In Figure (3.11 c) the ZnSe particles show agglomeration between (100-600) nm.

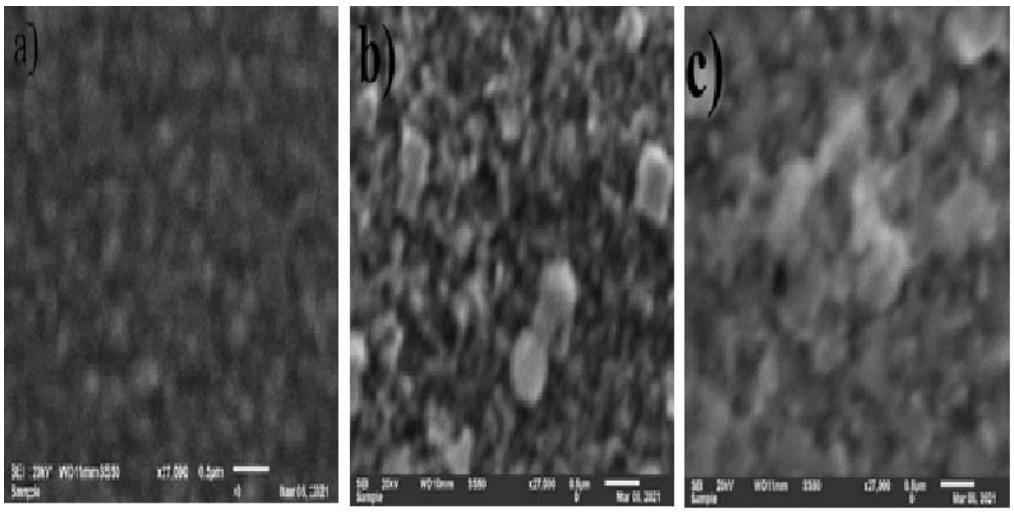

Figure 3.11: SEM images for ZnSe/FTO/glass thin films, a) ZnSe/FTO/glass, b) MWCNTs/ZnSe/FTO/glass and c) ZnSe/MWCNTs/FTO/glass.

3.2.5 ZnSe/FTO/glass thin film stability.

The stability of thin-films with highest conversion efficiency has been studied and the results are shown in Figure (3.12). Values of J_{SC} have been measured at applied potential (0 vs SCE), and recorded with time. The film modified with MWCNTs gives highest J_{sc} values and shows higher stability than others.

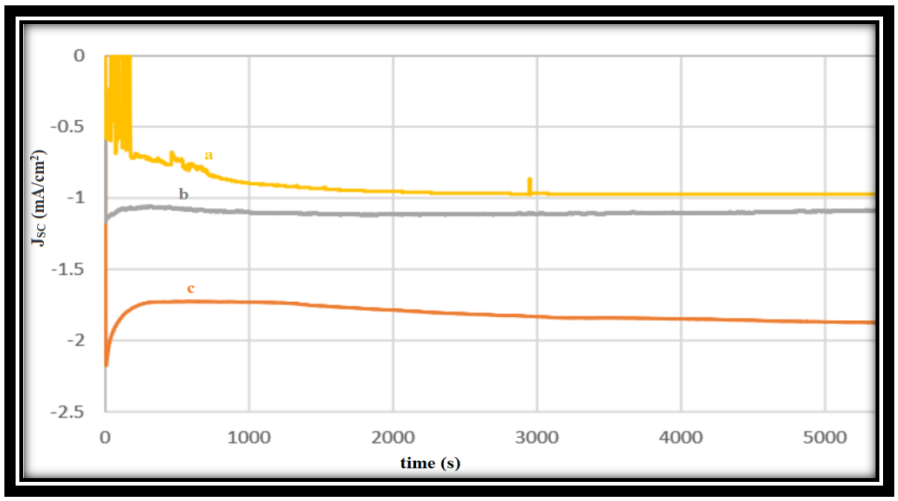

Figure 3.12: Plots of short circuit current density vs time for different films a) ZnSe/FTO/glass films nob-annealed, b) ZnSe/FTO/Glass annealed at 100 ºC rapidly cooled, and c) ZnSe/MWCNT/FTO/Glass. All measurements were conducted under PEC condition at room temperature.

3.3 Characteristic of ZnSe films electrodeposited on ITO/plastic.

ZnSe thin films have been electrodeposited on ITO/plastic substrates for the first time. ZnSe/ITO/Plastic film characteristics are described here for the first time.

3.3.1 XRD crystal study.

The XRD patterns of ZnSe/ITO/plastic thin films before and after annealing at 100 ºC are presented in Figure (3.13). All ZnSe films are polycrystalline with hexagonal crystal structure having orientations H (002), H (101), H (102) and H (110) as compared to literature [46]. The XRD patterns indicate that ZnSe thin films are mostly orientated toward (002) plane. The annealed film at 100 °C and slowly cooled has higher crystallinity than other films while the annealed film at 150 °C and slowly cooled has lower crystallinity than others. This confirms the effect of

higher temperatures on ZnSe thin film crystallinity. Annealing at high temperatures increase the kinetic energy and increases the disorder in the film.

XRD data have been used to measure the particle size of ZnSe using Scherrer equation, $D = k\lambda/\beta\cos\theta$ [42]. The average grain sizes were 15.87 nm (non-annealed), 16.18 nm (annealed at 100 °C, quickly cooled), 16.16 nm (annealed at 100 °C, slowly cooled), 16.52 nm (annealed at 150 °C, quickly cooled) and 17.32 nm (annealed at 150 °C, slowly cooled). The results show only little sintering at 100 °C and more sintering at 150 °C. With rapid cooling there is less sintering while with slow cooling the film is exposed to heat for longer time and more sintering.

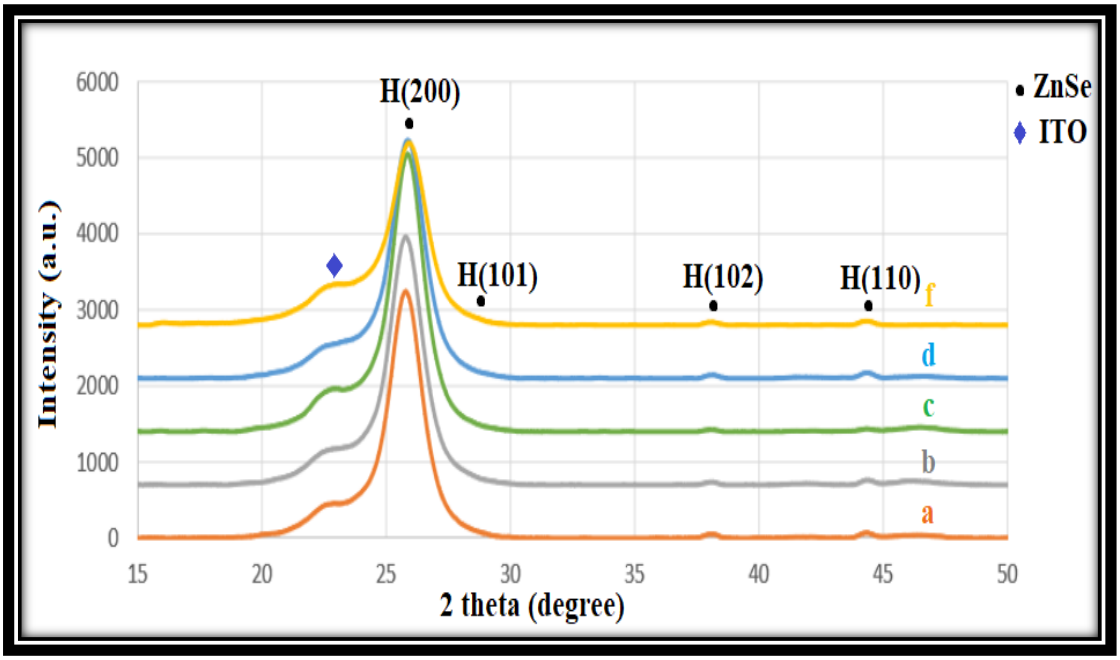

Figure 3.13: XRD patterns measured for ZnSe thin films electrodeposited on ITO/plastic. a) non-annealed, b) annealed at 100 °C, quickly cooled, c) annealed at 100 °C and slowly cooled, d) annealed at 150 °C, quickly cooled and f) annealed at 150 °C, slowly cooled.

3.3.2 Electronic absorption spectra.

3.3.2.1 The effect of deposition time on ZnSe/FTO/glass film electronic absorption spectra.

The electronic absorption spectra of the ZnSe/ITO/plastic thin films deposited in various deposition times are presented in Figure (3.14). Figure (3.14) shows that the highest absorption is for the film prepared in 30 minutes because the surface of the film deposited in 30 min was more uniform and smoother than the others, there are many interferences effect because ITO is conductive so should be highly reflecting, also because ZnSe has a high refractive index there can be an optimal thickness so there is no linear increase of absorbance with the film thickness and the optimal thickness here for the film deposited in 30 min.

Values of band gaps are summarized in Table (3.9). The band gap values are between (2.82-3.05) eV, which are higher than the band gap value for bulk ZnSe (2.7) eV.

The variation of band gap values confirms the effect of the deposition time on the average particle size. The band gaps decreased with increasing the deposition time due to increase the film thickness. However, when the deposition time was increased to 60 minutes, the band gap increased, due to presence of more impurities.

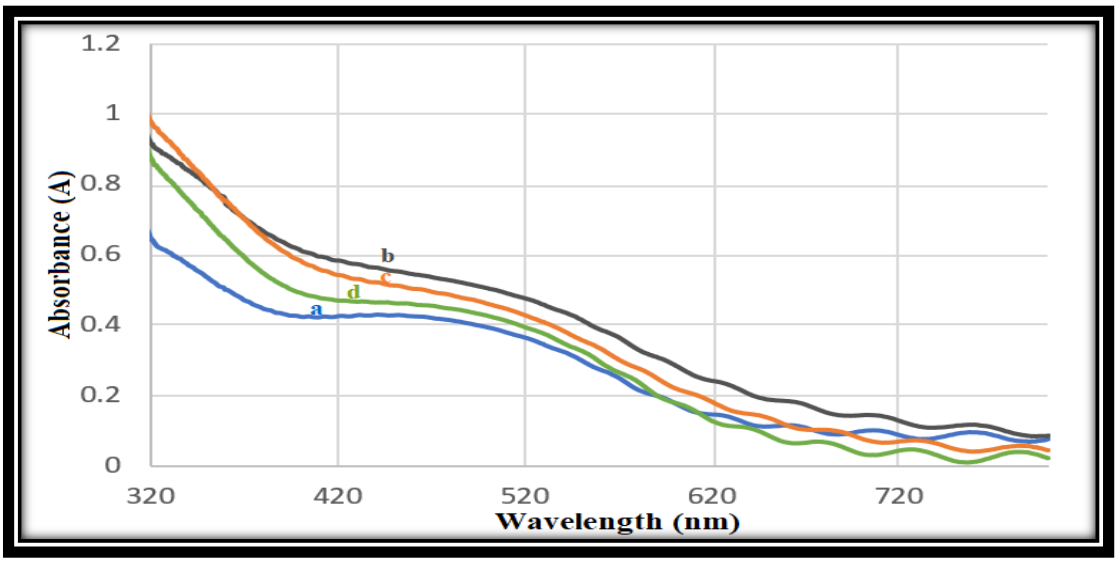

Figure 3.14: Optical absorption spectra measured for ZnSe thin film electrode deposited on ITO/plastic in various times, a) 15 min b) 30 min c) 45 min and d) 60 min.

Table 3.9: Values of optical band gaps for ZnSe/ITO/plastic electrodeposited in different time.

Sample	Deposition time (min)	E_{bg} (eV)	λ_{bg} (nm)
a	15	2.92	424
b	30	2.89	429
c	45	2.82	440
d	60	3.05	407

3.3.2.2 The effect of annealing temperature and cooling rate on ZnSe/ITO/plastic thin film electronic absorption spectra.

The prepared ZnSe/ITO/plastic thin films were annealed at (100 ºC and 150 ºC) and cooled slowly and quickly. Figure (3.15) shows the electronic absorption spectra of the prepared ZnSe thin films annealed at (100 ºC and 150 ºC) and cooled at different rates (slow and fast). The Figure shows that the annealed films at 100 ºC have better absorption spectra than the non-annealed film. The annealed film at 100 ºC with fast cooling has better

spectrum than the slowly cooled film. Annealing at 150 °C lowers the absorption spectra for the film.

Table (3.10) summarizes values for optical band gaps and absorption band gaps. The band gap values are lower for the films annealed at 150 ºC than annealed at 100 °C due to larger particle sizes and sintering. The films cooled slowly have lower the band gap values because they are exposed to heat for longer time with more sintering.

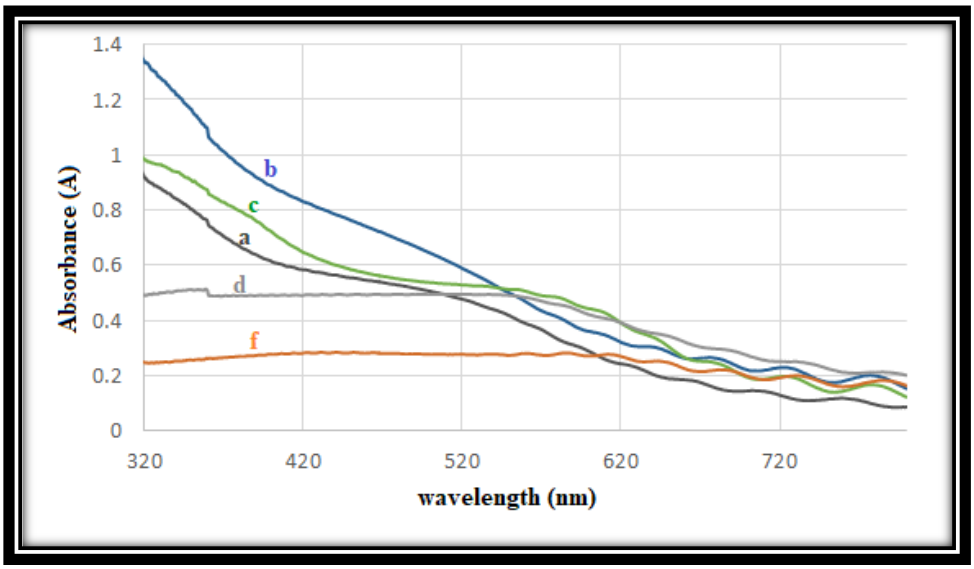

Figure 3.15: Optical absorption spectra measured for ZnSe thin film electrodes deposited on ITO/plastic and a) non-annealed b) annealed (100 ºC) rapidly cooled c) annealed (100 ºC) slowly cooled d) annealed (150 ºC) rapidly cooled and f) annealed (150 ºC) slowly cooled.

Table 3.10: Effect of annealing and cooling rate on optical band gap for ZnSe/ITO/plastic.

Sample	**description**	**E_{bg} (eV)**	**λ_{bg} (nm)**
a	Non-annealed	2.89	429
b	annealed at 100 °C, quenched	2.22	559
c	annealed at 100 °C, slowly	2.30	539
d	annealed at 150 °C, quenched	1.64	756
f	annealed at 150 °C, slowly	1.51	821

3.3.3 PEC measurement for ZnSe/ITO/Plastic thin films.

The photo-electrochemical characteristics of the prepared films have been studied. The photo J-V plots for films prepared under different conditions are measured.

3.3.3.1 Effect of deposition time on the J-V for ZnSe/ITO/plastic thin films.

Figure (3.16) shows the photo J-V plots for ZnSE/ITO/Plastic films deposited in different times. The conductivity for all films is p-type. The results of the Figure are summarized in table (3.11).

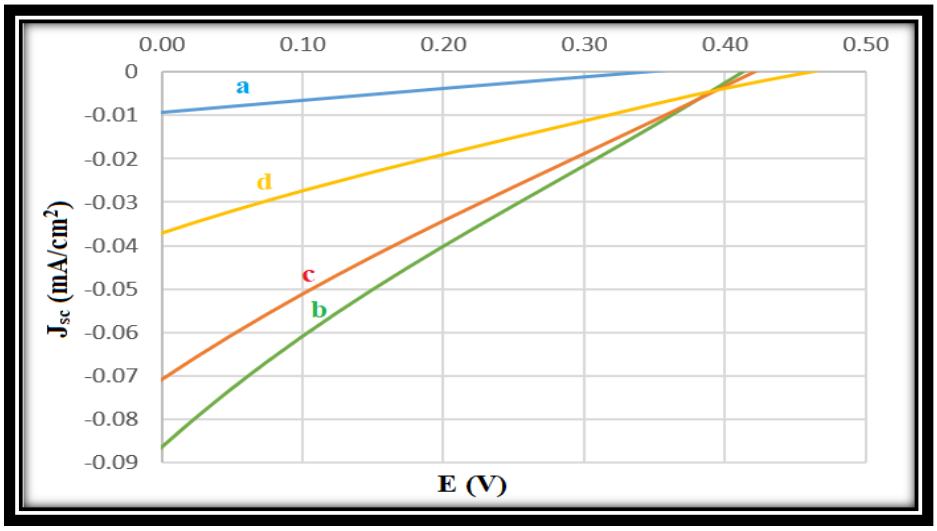

Figure 3.16: Photo J-V plots for the prepared ZnSe/ITO/plastic films deposited in a) 15, b) 30, c) 45 and d) 60 min.

Table 3.11: PEC characteristics for ZnSe/ITO/plastic films deposited in different times.

Sample	Deposition time (min)	[a] V_{OC} (V)	[b] J_{SC} (mA/cm^2)	[c] η%	[d] FF%
a	15	0.34	-0.009	0.007%	19.0%
b	30	0.41	-0.086	0.087%	21.8%

c	45	0.42	-0.071	0.081%	23.5%
d	60	0.46	-0.037	0.043%	22.0%

[a] V_{OC} = *open-circuit voltage*

[b] J_{SC} = *short-circuit* **current** *density*

[c] η *(%) = conversion efficiency = [(maximum observed power density)/ (reach-in power density)] ×100%.*

[d] *FF = Fill factor = [(maximum observed power density)/*J_{sc}*×*V_{oc}*] ×100%.*

The prepared films showed low efficiency, compared to ZnSe/FTO/glass films, Table (3.3). This is due to higher conductivity of FTO/glass compared to ITO/plastic. The films prepared on ITO/plastic have wide band gap values as shown in Table (3.11), which means they cannot absorb light in wider visible range. The highest efficiency here is for the film prepared in 30 min (~η 0.086%).

3.3.3.2 Effects of annealing temperature and cooling rate on J-V for ZnSe/ITO/plastic thin films.

PEC properties for ZnSe thin film annealed at (100 ºC and 150 ºC) with different cooling rates (slow and fast) are measured**.** Photo J-V plots for thin films annealed at (100 ºC and 150 ºC) and cooled slowly and quickly are shown in the Figure (3.17). The results of the figure are summarized in Table (3.12).

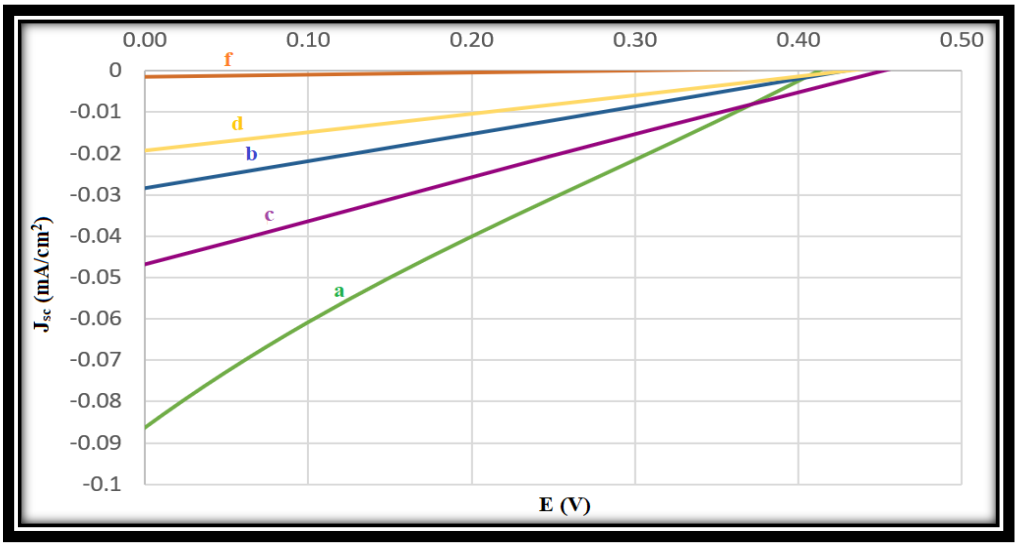

Figure 3.17: Photo J-V plots for ZnSe/ITO/plastic electrodes a) non-annealed, b) annealed at 100 ºC rapidly cooled c) annealed at 100 ºC slowly cooled d) annealed at 150 ºC rapidly cooled and f) annealed at 150 ºC slowly cooled.

Table 3.12: PEC characteristics for ZnSe/ITO/plastic thin films annealed at (100 ºC and 150 ºC) and cooling rate.

sample	description	[a] V_{OC} (V)	[b] J_{SC} (mA/cm^2)	[c] η%	[d] FF%
a	Non-annealed	0.41	-0.086	0.087%	21.3%
b	annealed at 100 °C, quickly cooled	0.43	-0.029	0.029%	16.0%
c	annealed at 100 °C, Slowly cooled	0.45	-0.047	0.066%	21.0%
d	annealed at 150 °C, quickly cooled	0.42	-0.019	0.022%	17.4%
f	annealed at 150 °C, Slowly cooled	0.35	-0.001	0.0017%	42.8%

[a] V_{OC} = *open-circuit voltage*

[b] J_{SC} = *short-circuit* current *density*

[c] η *(%) = conversion efficiency = [(maximum observed power density)/ (reach-in power density)] ×100%.*

[d] *FF = Fill factor = [(maximum observed power density)/*J_{sc}×V_{oc}*] ×100%.*

The non-annealed film gives better effeciancy (0.086%) than annealed films. The films annealed at 100 °C (0.029%, 0.066%) are better than films annealed at 150 °C (0.022%, 0.0017%) for rapid and slow cooling respectively. Here, PEC study for non-annealed film showed better than for annealed films. The efficiency result for annealed films at 100 °C does not correlate with XRD and electronic absorption spectrum results. This is because the ECD layer is uniform without annealing. Annealing at low temperature may cause a slight disorder in the particles. Annealing at higher temperatures (150 °C), with increased kinetic energy, further increases the disorder in the particles. With rapid cooling the film is expose to heat for shorter time with less disorder, while slow cooling particularly at high temperature increases the disorder and degradation of ZnSe layer and destruction of atomic network structure [53,54].

3.3.4 SEM images for ZnSe/ITO/plastic thin films.

SEM surface images have been measured for ZnSe/ITO/plastic after annealing at 100 ºC and slow cooling, Figure (3.18). The Figure shows agglomeration with nonuniform size between (50-600) nm.

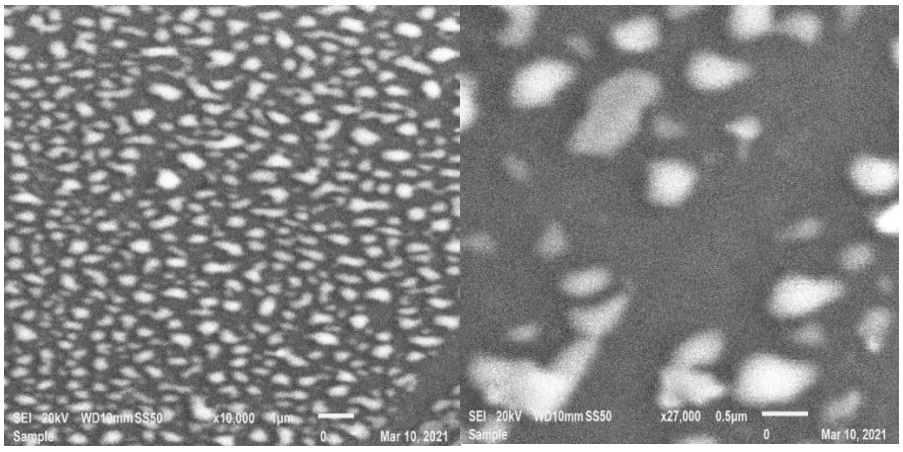

Figure 3.18: SEM images for ZnSe/ITO/plastic thin fim annealed at 100 °C and slowly cooled.

Conclusions

The ECD technique has been used to prepare ZnSe thin films on FTO/glass and on ITO/plastic.

1. The ZnSe thin film deposited on FTO/glass gives higher efficiency than the film deposited on ITO/plastic.
2. Non-annealed film showed higher efficiency than annealed films.
3. Modified the ZnSe thin film with MWCNTs enhanced their PEC characteristics and stability under PEC condition.

Suggestions for Future Work:

1. Prepare ZnSe thin films using electrochemical followed by chemical bath deposition.
2. Coating ZnSe thin films with different electro-active polymers.
3. Doping the ZnSe thin films with different metals
4. Electrodeposition of other type of semiconductors (CuS, CuSe, CdSe….) on ITO/plastic.
5. Pre-deposited of other types of semiconductors with MWCNTs.

References.

- D. J. Arent, A. Wise, and R. Gelman, "**The status and prospects of renewable energy for combating global warming,**" Energy Economics, vol. 33, pp. 584-593, 2011.
- R. R. Hernandez, S. Easter, M. L. Murphy-Mariscal, F. T. Maestre, M. Tavassoli, E. B. Allen, et al., "**Environmental impacts of utility-scale solar energy**," Renewable and Sustainable Energy Reviews, vol. 29, pp. 766-779, 2014.
- Z. Şen, "**Solar energy in progress and future research trends**," Progress in energy and combustion science, vol. 30, pp. 367-416, 2004.
- Card, K. Fitch, D. Kelly, Ch. Kemker and K. Rose, **Solar Radiation & Photosynthetically Active Radiation**, https://www.fondriest.com/environmental-measurements/parameters/weather/photosynthetically-active-radiation/#PAR7 (accessed on October 2020)
- M. Aman, K. Solangi, M. Hossain, A. Badarudin, G. Jasmon, H. Mokhlis, et al., "A review of Safety, **Health and Environmental (SHE) issues of solar energy system**," *Renewable and Sustainable Energy Reviews,* vol. 41, pp. 1190-1204, 2015.
- N. Kannan and D. Vakeesan, "**Solar energy for future world:-A review**," *Renewable and Sustainable Energy Reviews,* vol. 62, pp. 1092-1105, 2016.

- S. Ashok, **Solar Energy**, https://www.britannica.com/science/solar-energy (accessed in October 2020)
- **Semiconductors in everyday life**, https://www.hitachihightech.com/global/products/device/semiconductor/life.html (accessed in October 2020)
- R. E. Hummel, **Electronic properties of materials**: Springer Science & Business Media, 2011
- S.Byrnes, **Clean Energy**, http://cleanenergywiki.org/index.php?title=Band-gap (accessed in October 2020)
- **Semiconductors,** https://jimmeijer.com/band-gap-of-silicon-energy-band-in-semiconductor/ (accessed in October 2020)
- J.-N. Chazalviel, A. Belaıdi, M. Safi, F. Maroun, B. Erne, and F. Ozanam, "**In situ semiconductor surface characterisation: a comparative infrared study of Si, Ge and GaAs**," *Electrochimica Acta*, vol. 45, pp. 3205-3211, 2000.
- V. S. Raut, C. D. Lokhande, and V. V. Killedar, "**Photoelectrochemical studies on electrodeposited indium doped CdSe thin films using aqueous bath,"** *Journal of Electroanalytical Chemistry*, vol. 788, pp. 137-143, 2017.
- S. Yoon, I. Huh, J.-H. Lim, and B. Yoo, **"Annealing effects on electrical and optical properties of ZnO thin films synthesized by**

the electrochemical method," *Current Applied Physics,* vol. 12, pp. 784-788, 2012.

- J. Chaudhari and U. Joshi, **"Synthesis and physical properties of low cost, non toxic, earth abundant p-type CuInS2 thin film as absorber layer for photovoltaic application,"** *Materials Today: Proceedings,* vol. 5, pp. 23434-23438, 2018.
- S. Dridi, N. Bitri, and M. Abaab, **"Synthesis of quaternary Cu2NiSnS4 thin films as a solar energy material prepared through «Spray» technique,"** *Materials Letters,* vol. 204, pp. 61-64, 2017.
- J. S. Galsin, **Solid State Physics: An Introduction to Theory**: Academic Press, 2019.
- K. Miyata, K. Kobashi, and D. L. Dreifus, "**Rectifying diodes with a metal/intrinsic semiconductor/semiconductor structure using polycrystalline diamond films,"** *Diamond and Related Materials,* vol. 2, pp. 1107-1111, 1993.
- A.Maurya, **Fermi Level of intrinsic Semiconductor**, \https://sites.google.com/site/puenggphysics/home/unit-5/fermi-level-of-intrinsic-and-extrinsic-semiconductor (accessed in October 2020)
- A.-R. Nour Nayef, "**CdSe Thin Film Photoelectrochemical Electrodes: Combined Electrochemical and Chemical Bath Depositions**," 2015.
- H. O. Finklea, "**Semiconductor electrodes**," 1988.

- Z. Salameh, **Renewable energy system design**: Academic Press, 2014.
- C. Sorrell, J. Nowotny, and S. Sugihara, **Materials for energy conversion devices**: Elsevier, 2005.
- Ma'ruf, **Electron Hole Pair**, http://www.villageinframe.com/electron-hole-pair/ (accessed in October 2020).
- K. Rajeshwar, P. Singh, and J. DuBow, "**Energy conversion in photoelectrochemical systems—a review**," *Electrochimica Acta,* vol. 23, pp. 1117-1144, 1978.
- G. Debernardi and C. Carlesi, "**Chemical-electrochemical approaches to the study passivation of chalcopyrite,"** *Mineral Processing and Extractive Metallurgy Review*, vol. 34, pp. 10-41, 2013.
- K. W. Frese, H.O.F., ***Semiconductor Electrodes*. 15th ed**. 1988, Amsterdam: Elsevier.
- J. Portier, H. Hilal, I. Saadeddin, S. Hwang, M. Subramanian, and G. Campet, **"Thermodynamic correlations and band gap calculations in metal oxides,"** *Progress in Solid State Chemistry,* vol. 32, pp. 207-217, 2004.
- K. Rajeshwar, **"Fundamentals of semiconductor electrochemistry and photoelectrochemistry,"** *Encyclopedia of Eelectrochemistry,* vol. 6, pp. 1-53, 2007.

- T. D. Lee and A. U. Ebong, **"A review of thin film solar cell technologies and challenges,"** *Renewable and Sustainable Energy Reviews*, vol. 70, pp. 1286-1297, 2017.
- M. Benelmekki and A. Erbe, **"Nanostructured thin films–background, preparation and relation to the technological revolution of the 21st century,"** in *Frontiers of Nanoscience*. vol. 14, ed: Elsevier, 2019, pp. 1-34.
- Zyoud, I. Saa'deddin, S. Khudruj, Z. M. Hawash, D. Park, G. Campet, *et al.*, **"CdS/FTO thin film electrodes deposited by chemical bath deposition and by electrochemical deposition: a comparative assessment of photo-electrochemical characteristics,"** *Solid State Sciences*, vol. 18, pp. 83-90, 2013.
- R. Khalfi, D. Talantikite-Touati, A. Tounsi, and H. Merzouk, **"Effect of deposition time on structural and optical properties of ZnSe thin films grown by CBD method,"** *Optical Materials*, vol. 106, p. 109989, 2020.
- Mehta, G. Saini, J. M. Abbas, and S. Tripathi, **"Effect of deposition parameters on structural, optical and electrical properties of nanocrystalline ZnSe thin films,"** *Applied Surface Science*, vol. 256, pp. 608-614, 2009.
- S. Thirumavalavan, K. Mani, and S. Sagadevan, **"A study of structural, morphological, optical and electrical properties of Zinc**

Selenide (ZnSe) thin film," *Materials Today: Proceedings,* vol. 3, pp. 2305-2314, 2016.

- M. Hasaneen, Z. Alrowaili, and W. Mohamed, **"Structure and optical properties of polycrystalline ZnSe thin films: validity of Swanepol's approach for calculating the optical parameters,"** *Materials Research Express,* vol. 7, p. 016422, 2020.
- Q. Zhang, H. Li, Y. Ma, and T. Zhai, **"ZnSe nanostructures: synthesis, properties and applications,"** *Progress in Materials Science,* vol. 83, pp. 472-535, 2016.
- S. Chuhadiya, R. Sharma, S. Patel, S. Chander, M. Kannan, and M. Dhaka, **"Thermal annealing induced physical properties of ZnSe thin films for buffer layer in solar cells,"** *Physica E: Low-Ddimensional Systems and Nanostructures,* vol. 117, p. 113845, 2020.
- J. Sharma and S. Tripathi, **"Effect of deposition pressure on structural, optical and electrical properties of zinc selenide thin films,"** *Physica B: Condensed Matter,* vol. 406, pp. 1757-1762, 2011.
- G. Riveros, H. Gomez, R. Henrıquez, R. Schrebler, R. Marotti, and E. Dalchiele, **"Electrodeposition and characterization of ZnSe semiconductor thin films,"** *Solar Eenergy Materials and Solar Cells,* vol. 70, pp. 255-268, 2001.
- Shirmardi, M. A. M. Teridi, H. R. Azimi, W. J. Basirun, F. Jamali-Sheini, and R. Yousefi, **"Enhanced photocatalytic performance of ZnSe/PANI nanocomposites for degradation of organic and**

inorganic pollutants," *Applied Surface Science*, vol. 462, pp. 730-738, 2018.

- J. Wang, H. Feng, W. Fan, K. Chen, and Q. Yang, **"Wet-chemical synthesis and optical property of ZnSe nanowires by Ag 2 Se-catalyzed growth mechanism,"** *Advances in Materials Physics and Chemistry*, vol. 2013, 2013.
- H. Xiao, R. Liang, O. Spires, H. Wang, H. Wu, and Y. Zhang, **"Evaluation of surface and subsurface damages for diamond turning of ZnSe crystal,"** *Optics express*, vol. 27, pp. 28364-28382, 2019.
- S. Muthumari, G. Devi, P. Revathi, R. Vijayalaks, and C. Sanjeevira, **"Structural Investigation of Zinc Selenide Thin Films,"** *Journal of Applied Sciences*, vol. 12, pp. 1722-1725, 2012.
- L. Mohan, N. Sisupalan, K. Ponnusamy, and S. Sadagopalan, **"One Step Synthesis and Characterization of ZnO–ZnSe Heterostructures by Chemical Precipitation and Its Solar Photocatalytic Activity,"** *Journal of Inorganic and Organometallic Polymers and Materials*, vol. 30, pp. 2626–2632, 2020.
- P. N. Bartlett, D. Cook, C. K. de Groot, A. L. Hector, R. Huang, A. Jolleys, *et al.*, **"Non-aqueous electrodeposition of p-block metals and metalloids from halometallate salts,"** *RSC advances*, vol. 3, pp. 15645-15654, 2013.

- L. H. Lalasari, T. Arini, L. Andriyah, F. Firdiyono, and A. H. Yuwono, **"Electrical, optical and structural properties of FTO thin films fabricated by spray ultrasonic nebulizer technique from SnCl4 precursor,"** in *AIP Conference Proceedings*, 2018, p. 020001.
- S. Abu Alrob, **Recycling CdSe-Based Thin Film Solar Cells**, MSc Thesis, An-Najah National University, Nablus, Palestine, 2019.
- K. A. Q. Murtada, **"Combined Electrochemical and Chemical Bath Deposition Techniques to Prepare CuSe Thin Film Electrodes for Solar Energy Purposes**, MSc Thesis, An-Najah National University, Nablus, Palestine,2014.
- G. Riveros, H. Gómez, R. Henríquez, R. Sshrebler, R. Cordova, R. Marotti, *et al.*, **"Electrodeposition and characterization of ZnX (X= Se, Te) semiconductor thin films,"** *Boletín de la Sociedad Chilena de Química*, vol. 47, pp. 411-429, 2002.
- G. Riveros, H. Gomez, R. Henrıquez, R. Schrebler, R. Marotti, and E. Dalchiele, **"Electrodeposition and characterization of ZnSe semiconductor thin films,"** *Solar Energy Materials and Solar Cells*, vol. 70, pp. 255-268, 2001.
- Zyoud, R. S. AlKerm, R. S. Alkerm, D. Park, M. H. Helal, G. Campet, *et al.*, **"Enhanced PEC characteristics of pre-annealed CuS film electrodes by metalloporphyrin/polymer matrices,"** *Solar Energy Materials and Solar Cells*, vol. 144, pp. 429-437, 2016.
- Zyoud, I. Saa'deddin, S. Khudruj, Z. M. Hawash, D. Park, G. Campet, *et al.*, **"CdS/FTO thin film electrodes deposited by chemical bath deposition and by electrochemical deposition: a comparative**

assessment of photo-electrochemical characteristics," *Solid State Sciences,* vol. 18, pp. 83-90, 2013

- Salem, E. Saion, N. M. Al-Hada, H. M. Kamari, A. H. Shaari, and S. Radiman**, "Simple synthesis of ZnSe nanoparticles by thermal treatment and their characterization,"** *Results in Physics,* vol. 7, pp. 1175-1180, 2017.

Appendix

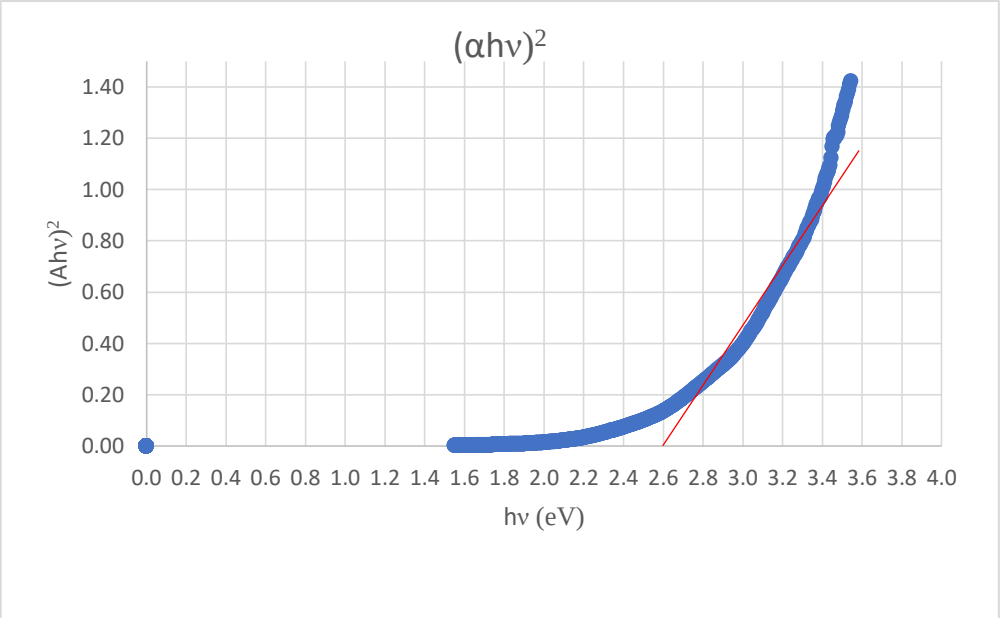

Figure (1) :Tauc Plot from UV-Vis analysis of ZnSe/FTO/glass film deposited in 15 min.

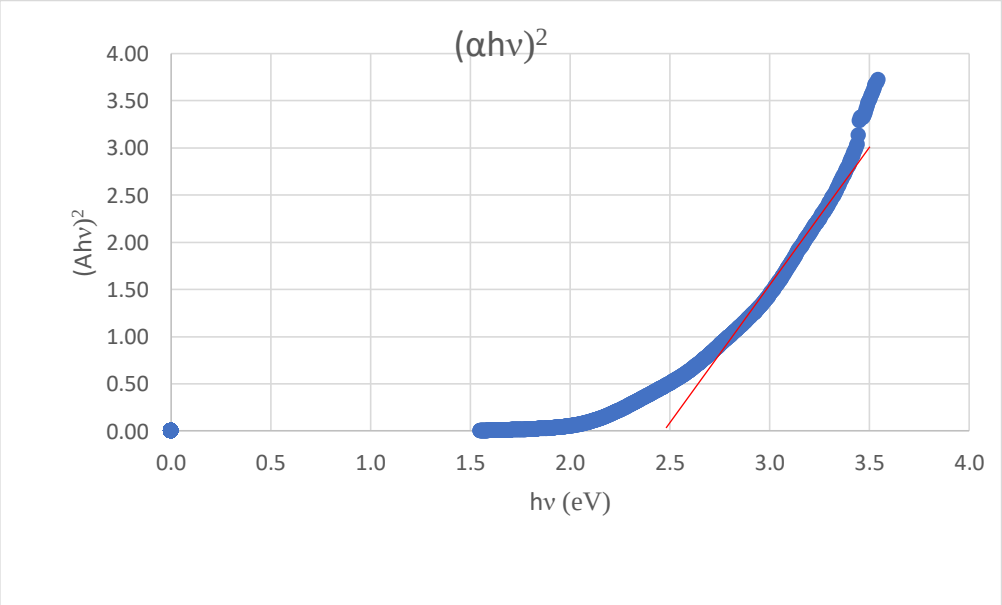

Figure (2) :Tauc Plot from UV-Vis analysis of ZnSe/FTO/glass film deposited in 30 min

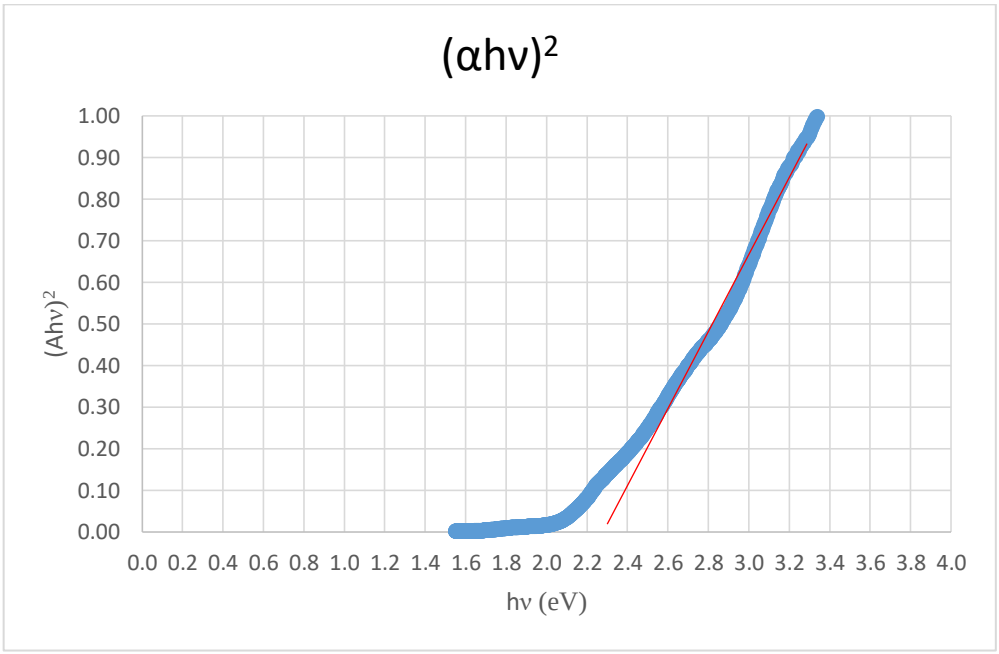

Figure (3) :Tauc Plot from UV-Vis analysis of ZnSe/FTO/glass film deposited in 45 min

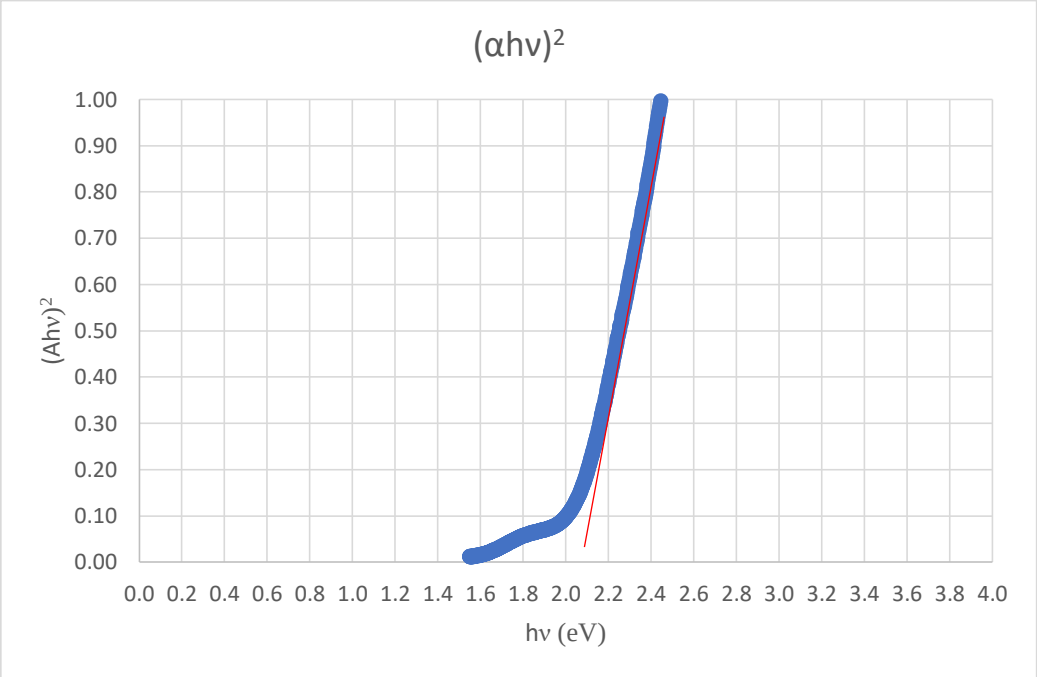

Figure (4) :Tauc Plot from UV-Vis analysis of ZnSe/FTO/glass film deposited in 60 min

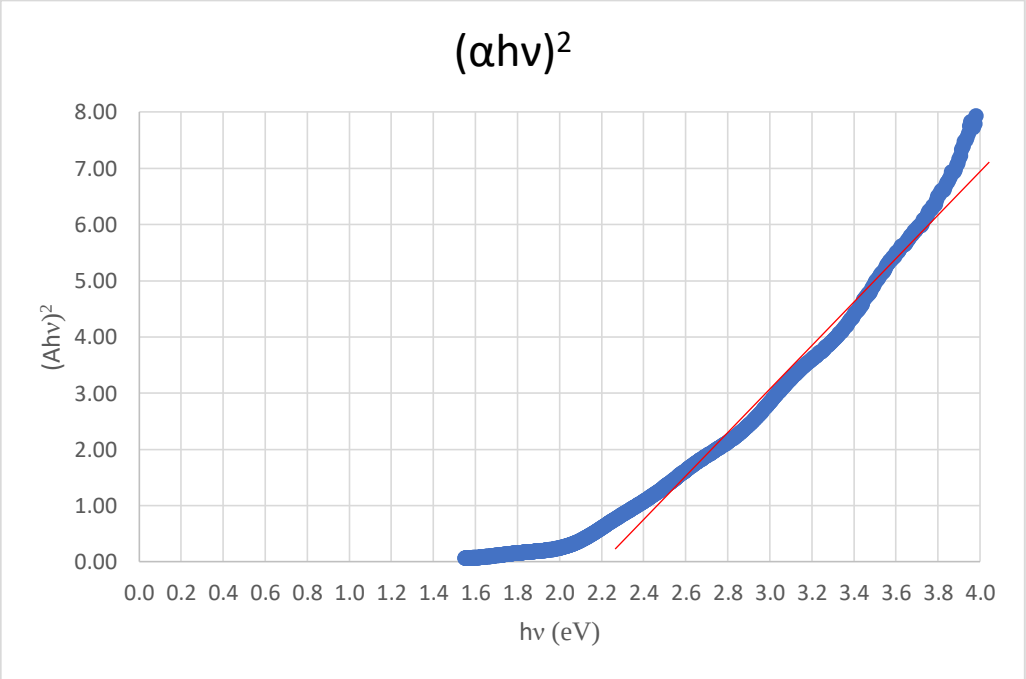

Figure (5) :Tauc Plot from UV-Vis analysis of ZnSe/FTO/glass film annealed at 100 °C, rapidly cooled.

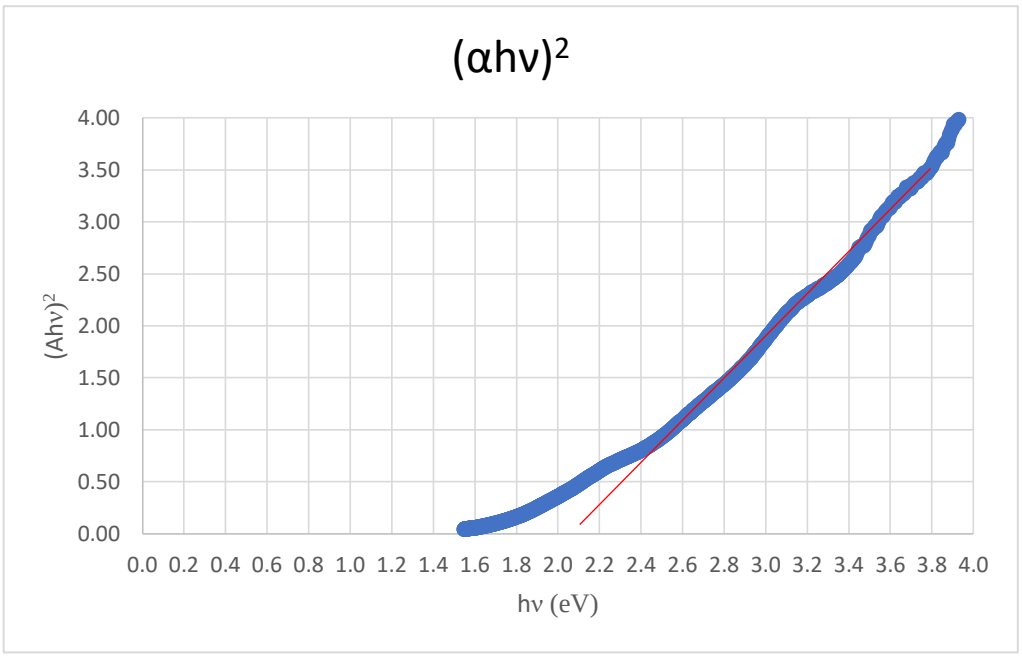

Figure (6) :Tauc Plot from UV-Vis analysis of ZnSe/FTO/glass film annealed at 100 °C, slowly cooled.

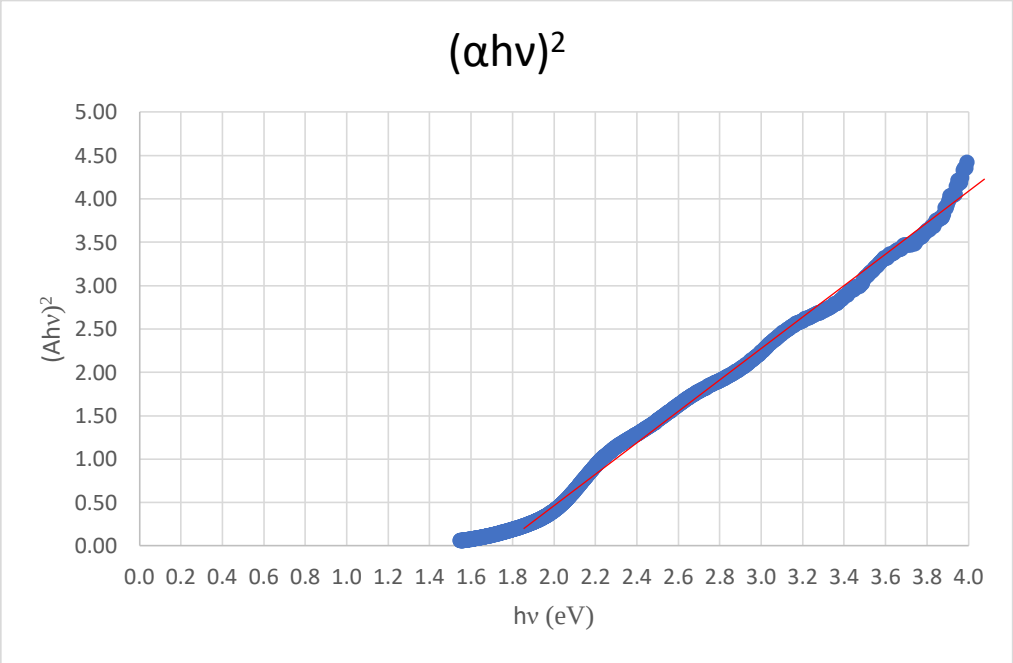

Figure (7) :Tauc Plot from UV-Vis analysis of ZnSe/FTO/glass film annealed at 150 °C, rapidly cooled.

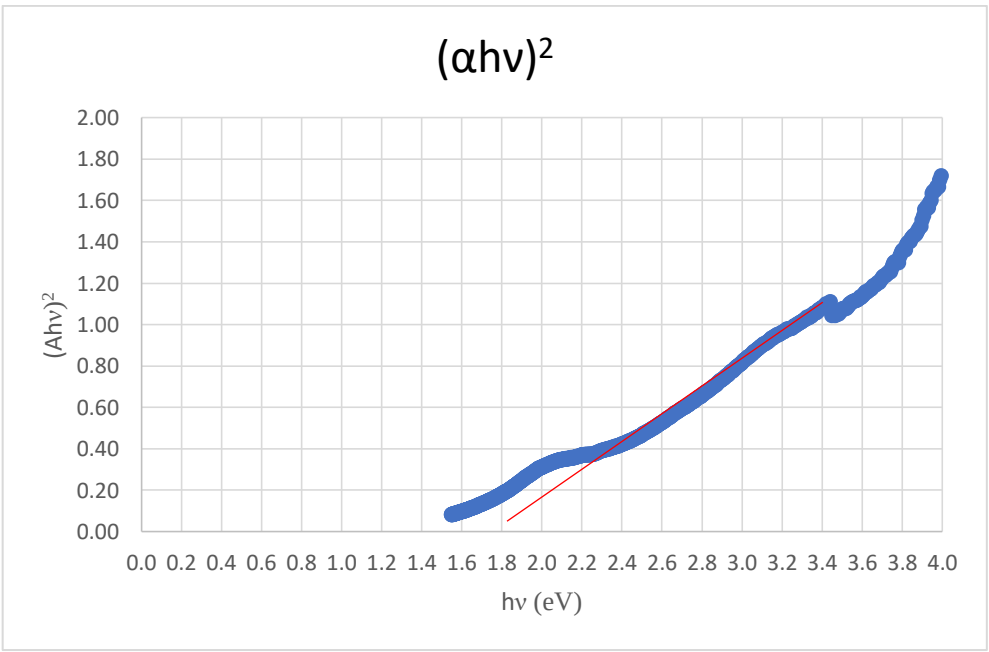

Figure (8) :Tauc Plot from UV-Vis analysis of ZnSe/FTO/glass film annealed at 150 °C, slowly cooled.

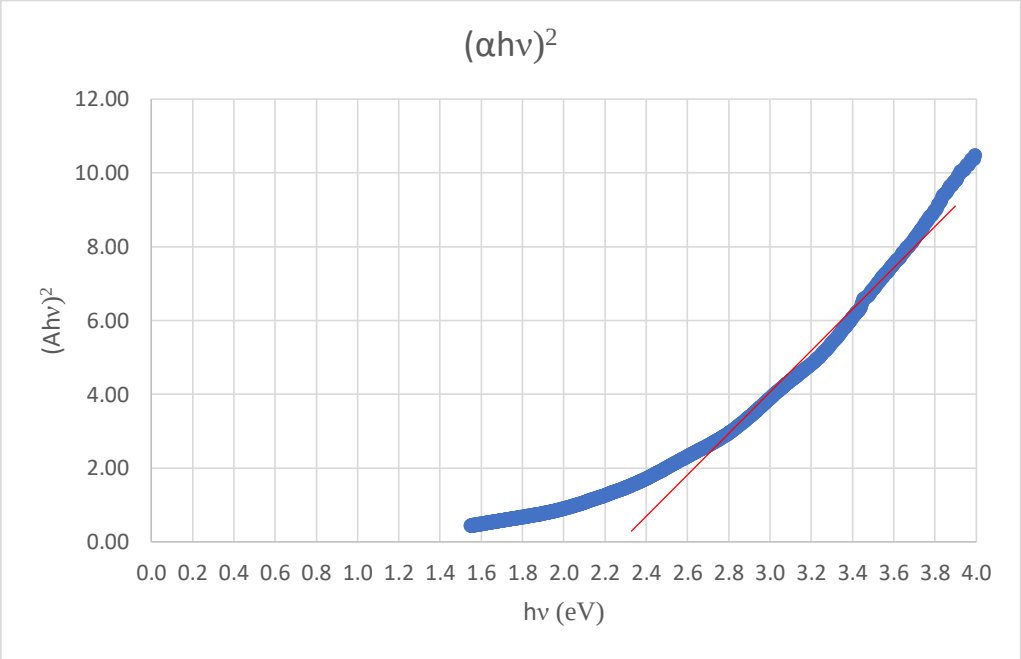

Figure (9) :Tauc Plot from UV-Vis analysis of ZnSe/MWCNT/FTO/glass film.

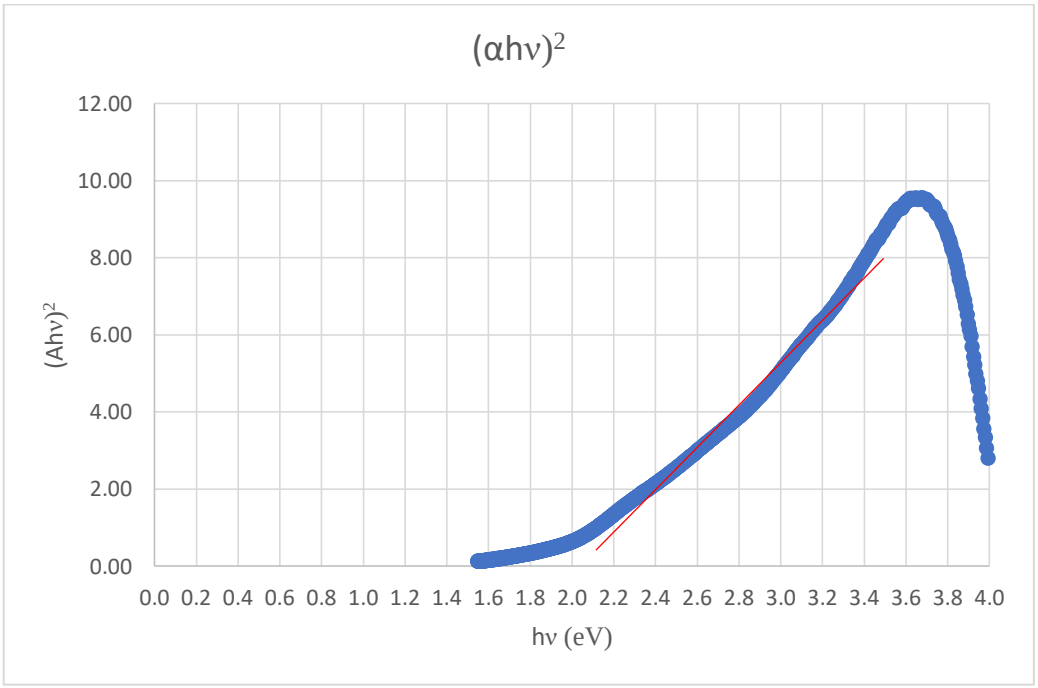

Figure (10) :Tauc Plot from UV-Vis analysis of MWCNT/ZnSe/FTO/glass film.

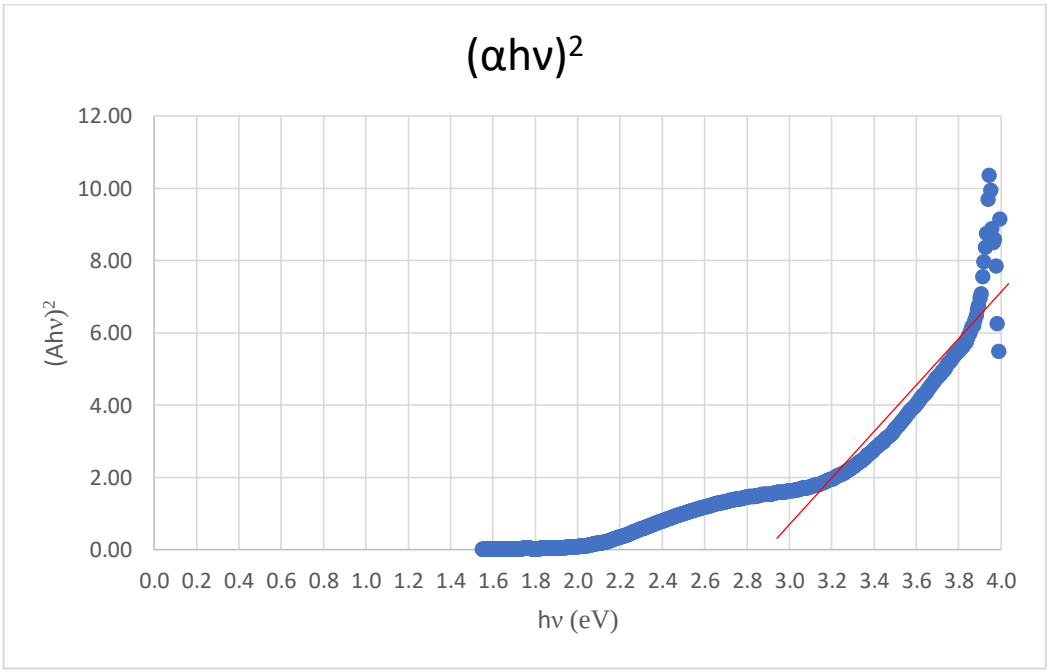

Figure (11) :Tauc Plot from UV-Vis analysis of ZnSe/ITO/plastic film deposited in 15 min.

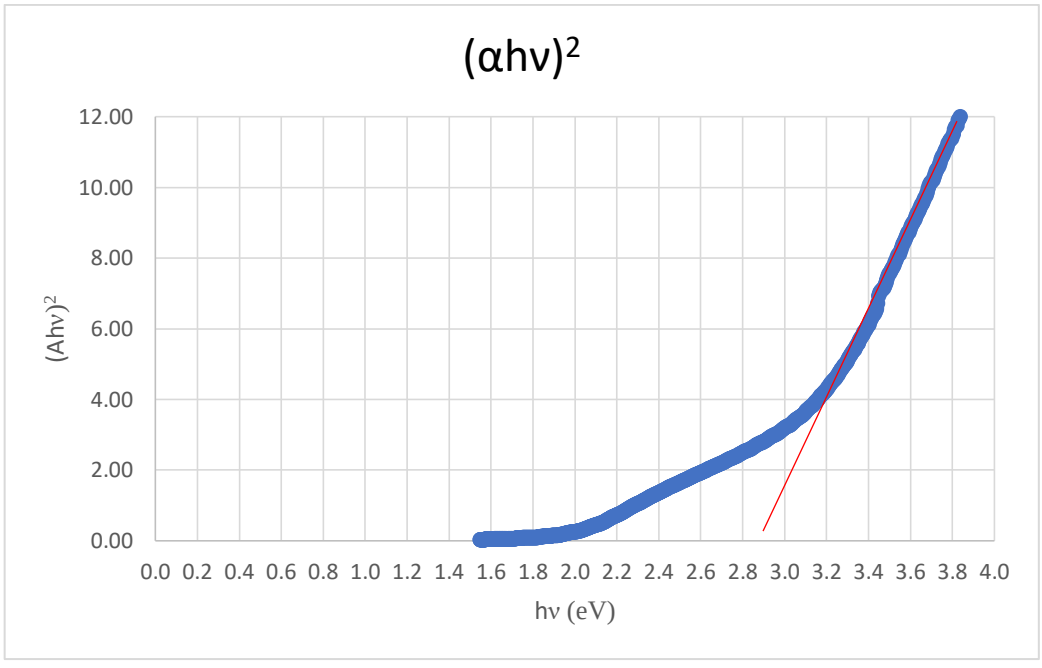

Figure (12) :Tauc Plot from UV-Vis analysis of ZnSe/ITO/plastic film deposited in 30 min.

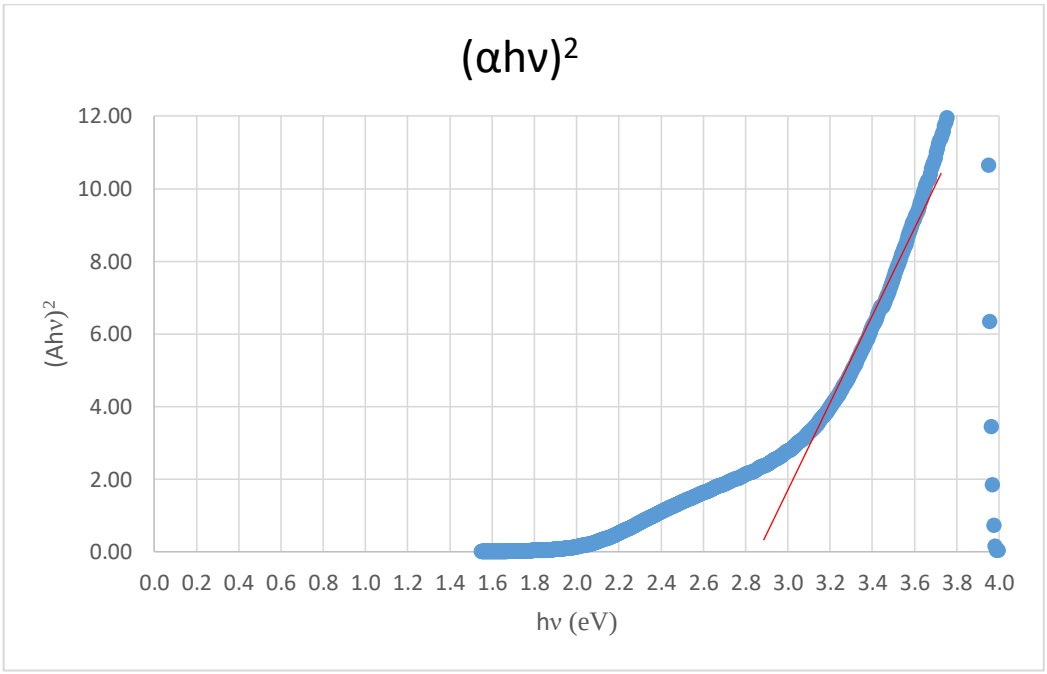

Figure (13) :Tauc Plot from UV-Vis analysis of ZnSe/ITO/plastic film deposited in 45 min.

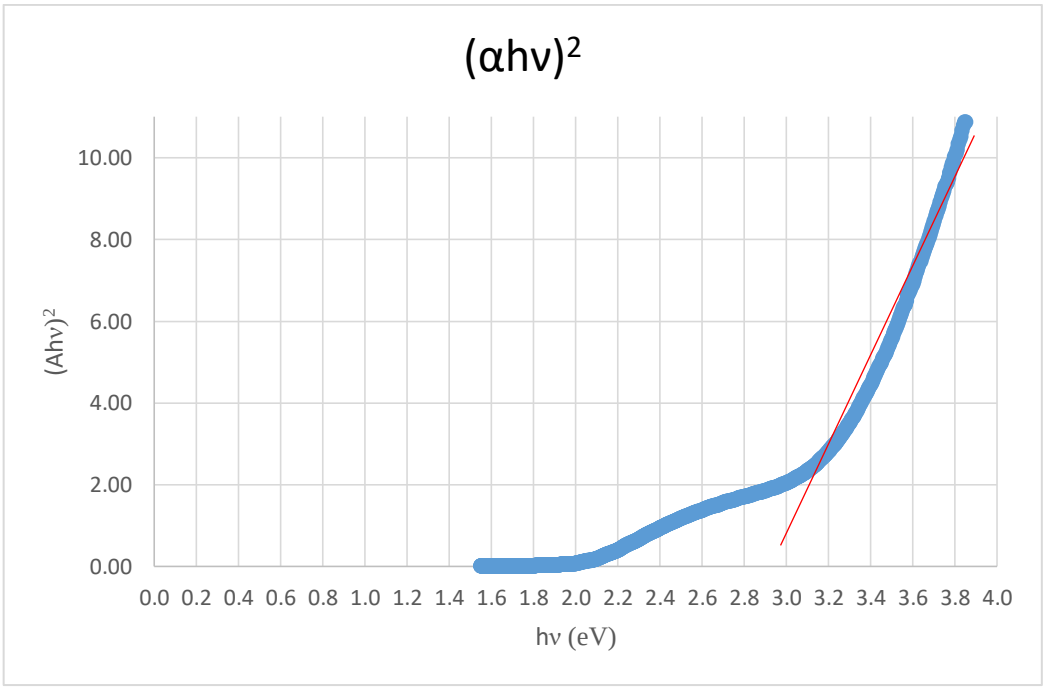

Figure (14) :Tauc Plot from UV-Vis analysis of ZnSe/ITO/plastic film deposited in 60 min.

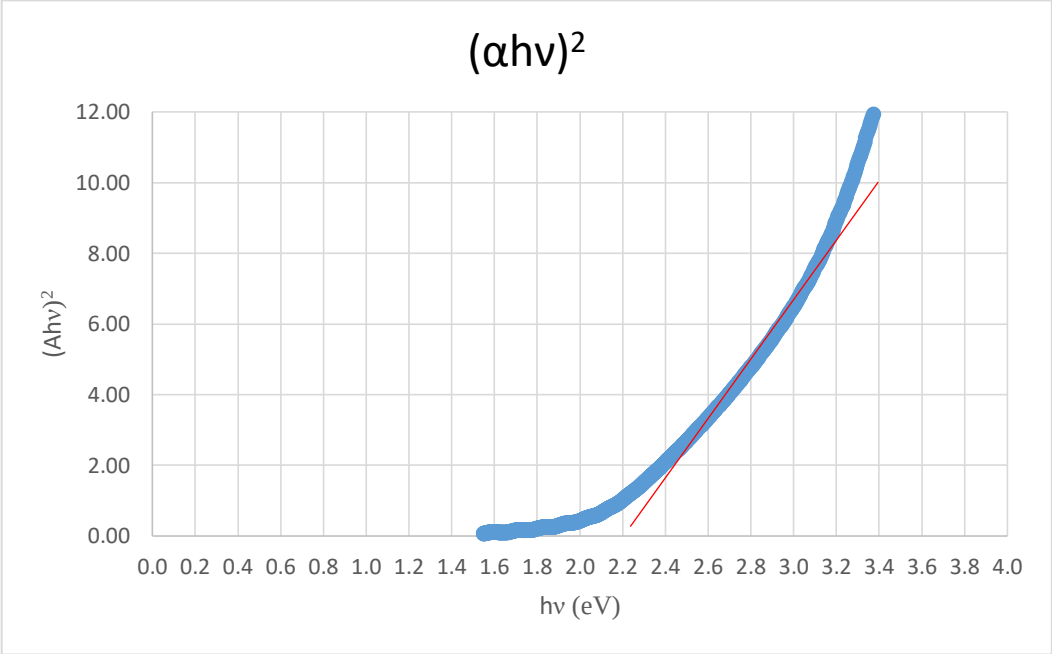

Figure (15) :Tauc Plot from UV-Vis analysis of ZnSe/ITO/plastic film annealed at 100 °C, rapidly cooled.

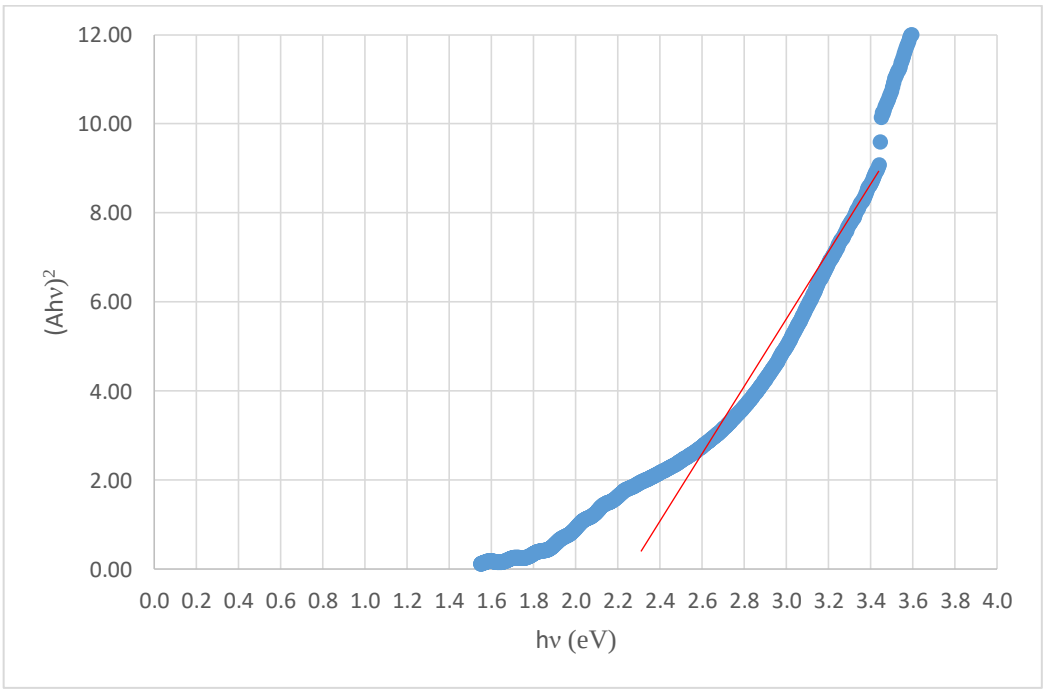

Figure (16) :Tauc Plot from UV-Vis analysis of ZnSe/ITO/plastic film annealed at 100 °C, slowly cooled.

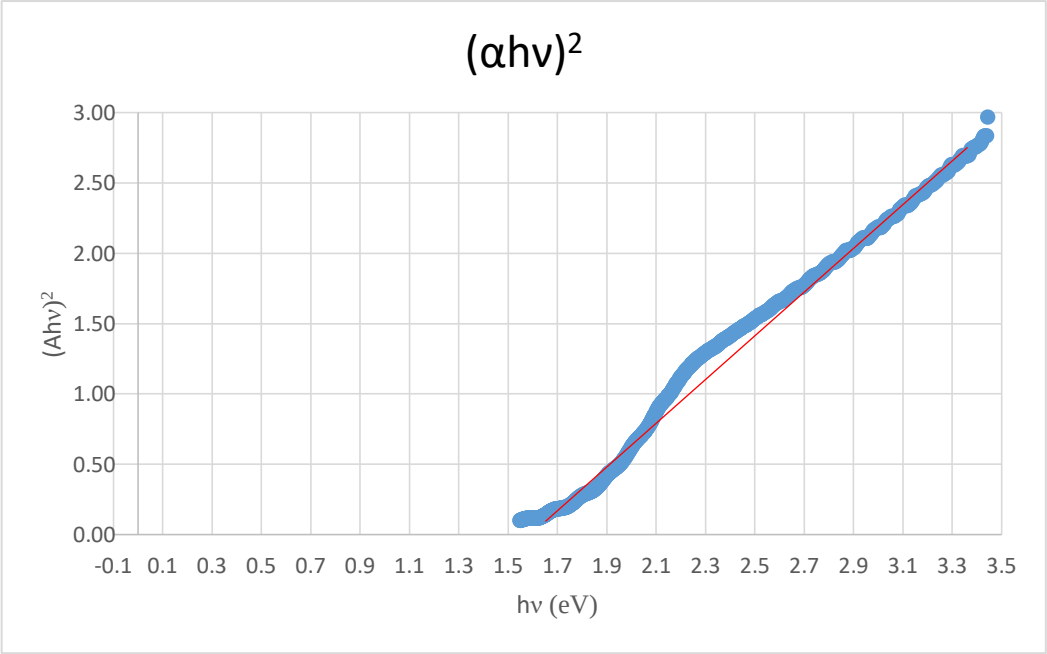

Figure (17) :Tauc Plot from UV-Vis analysis of ZnSe/ITO/plastic film annealed at 150 °C, rapidly cooled.

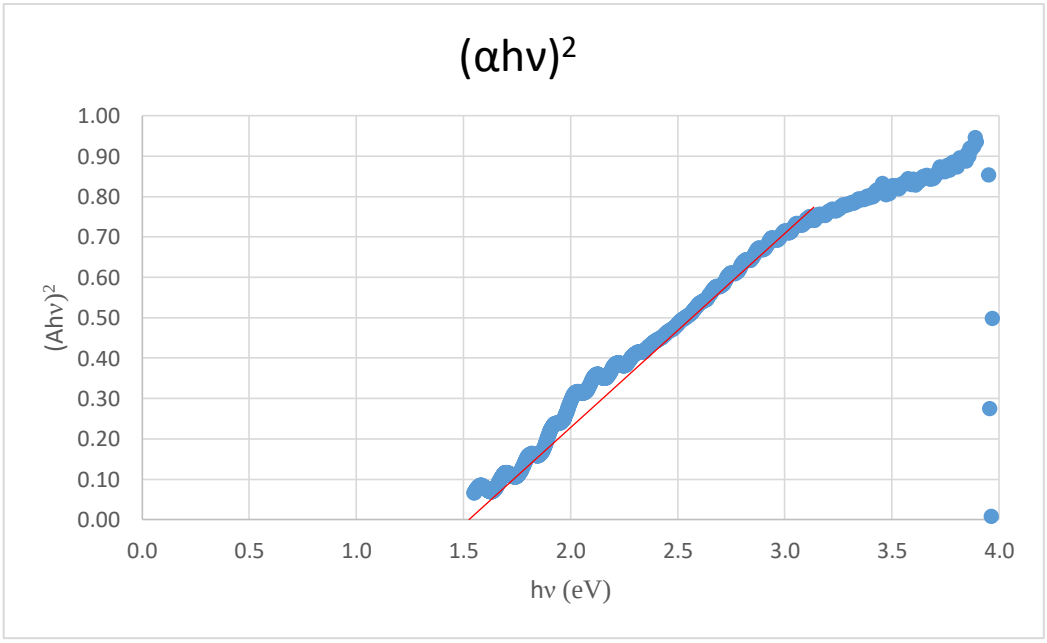

Figure (18) :Tauc Plot from UV-Vis analysis of ZnSe/ITO/plastic film annealed at 150 °C, slowly cooled.

جامعة النجاح الوطنية

كلية الدراسات العليا

انتاج أفلام نانوية مفيدة من ZnSe بالترسيب الكهربائي على شرائح الزجاج والبلاستيك الموصلة

إعداد

هبه مهند محمد غنام

إشراف

أ.د حكمت هلال

د. عاهد زيود

قدمت هذه الأطروحة استكمالاً لمتطلبات الحصول على درجة الماجستير في الكيمياء بكلية الدراسات العليا في جامعة النجاح الوطنية، نابلس – فلسطين.

2021

انتاج أفلام نانوية مفيدة من ZnSe بالترسيب الكهربائي على شرائح الزجاج والبلاستيك االموصلة

اعداد

هبة مهند محمد غنام

اشراف

أ.د حكمت هلال

د.عاهد زيود

الملخص

تم ترسيب الأقطاب الكهربائية ذات الأفلام الرقيقة ZnSe على نوعين من الشرائح الموصلة الشفافة ، الزجاج المغطاة بأكسيد القصدير المزود بالفلور (FTO) والشرائح البلاستيكية المغطاة بأكسيد القصدير المزود بالإنديوم (ITO) ، عن طريق الترسيب الكهروكيميائي (ECD). بعد ذلك تمت دراسة خصائص الأفلام المحضرة بتقنيات مختلفة (اطياف انحراف اشعة اكس (XRD) ، المسح المجهري الإلكتروني (SEM) وأطياف الامتصاص الإلكترونية). تمت دراسة تأثير زمن الترسيب ودرجة حرارة الشي (100 درجة مئوية و 150 درجة مئوية تحت غاز خامل) ومعدل التبريد (التبريد السريع والبطيء) والتعديل باستخدام (MWCNTs) على خصائص الفوتوكهروكيميائية(PEC) للافلام . افلام ZnSe لها موصلية من النوع p كما اظهرتها قياسات الفوتوكهروكيميائية.

تُظهر قياسات XRD أن الأفلام الرقيقة (ZnSe / FTO / glass) تضمنت جزيئات بحجم النانو مع بلورات مختلطة من النوع السداسي والمكعب ، في حين أن ZnSe / ITO/plastic تضمن بلورات من النوع السداسي فقط. أظهرت أطياف الامتصاص الإلكتروني للأغشية المحضرة علىFTO/ glass قيم فجوة نطاق تتراوح بين (2.6–2.4 eV) ، أما بالنسبة للأفلام المودعة على ITO/plastic فتتراوح قيم فجوة النطاق بين (2.9–3.1 eV). تقل قيمة فجوة النطاق مع ارتفاع درجات حرارة الشي. تظهر الأفلام المبردة بسرعة فجوة نطاق أعلى من تلك التي يتم تبريدها ببطء.

تعطي الأفلام المرسبة على FTO/glass كفاءة تحويل أعلى (0.84٪) من الأفلام المرسبة على ITO/plastic (0.087٪). أدى شي الأفلام الرقيقة من ZnSe إلى خفض خصائص PEC. تمت دراسة تأثير استخدام طبقات الأنابيب النانوية الكربونية متعددة الجدران (MWCNT) على أقطاب ZnSe / FTO / Glass. تم تقديم طبقة MWCNT بطريقتين مختلفتين: عن طريق الإدخال بين طبقة ZnSe وطبقة FTO((ZnSe/MWCNT /FTO/glass)، أو عن طريق طلاء ZnSe بـ MWCNT (MWCNT / ZnSe / FTO/glass). يُظهر (ZnSe / MWCNT / FTO/glass)s كفاءة تحويل أعلى (1.68٪) مقارنة بـ (0.84٪) لقطب(ZnSe FTO/glass). في هذه الحالة ، تتصرف طبقة MWCNT كعامل نقل شحنة بين طبقة ZnSe و FTO. يُظهر القطب الكهربي (MWCNT / ZnSe / FTO/glass) كفاءة تحويل أقل (0.61٪). ربما يرجع ذلك إلى قدرة طلاء MWCNT على منع الضوء الساقط من الوصول إلى سطح ZnSe